JOURNAL OF PETROLOGY | VOLUME 50 | NUMBER 4 | PAGES 685–723 | 2009 | doi:10.1093/petrology/egp017

Silicic Magmas in the Izu–Bonin Oceanic Arc and Implications for Crustal Evolution

YOSHIHIKO TAMURA[1,2]*, JAMES B. GILL[2], DARREN TOLLSTRUP[2], HIROSHI KAWABATA[1], HIROSHI SHUKUNO[1], QING CHANG[1], TAKASHI MIYAZAKI[1], TOSHIRO TAKAHASHI[1], YUKA HIRAHARA[1], SHUICHI KODAIRA[1], OSAMU ISHIZUKA[3], TOSHIHIRO SUZUKI[1], YUKARI KIDO[4], RICHARD S. FISKE[5] AND YOSHIYUKI TATSUMI[1]

[1]INSTITUTE FOR RESEARCH ON EARTH EVOLUTION (IFREE), JAPAN AGENCY FOR MARINE–EARTH SCIENCE AND TECHNOLOGY (JAMSTEC), YOKOSUKA 237-0061, JAPAN

[2]UNIVERSITY OF CALIFORNIA, SANTA CRUZ, CA 95064, USA

[3]INSTITUTE OF GEOSCIENCE, GEOLOGICAL SURVEY OF JAPAN/AIST, TSUKUBA 305-8567, JAPAN

[4]CENTER FOR DEEP EARTH EXPLORATION (CDEX), JAPAN AGENCY FOR MARINE–EARTH SCIENCE AND TECHNOLOGY, 3173-25 SHOWA-MACHI, KANAZAWA-KU YOKOHAMA, 236-0001, JAPAN

[5]SMITHSONIAN INSTITUTION, NMNH MRC-119, WASHINGTON, D.C. 20013-7012, USA

RECEIVED AUGUST 27, 2008; ACCEPTED MARCH 18, 2009
ADVANCE ACCESS PUBLICATION APRIL 15, 2009

Abundant rhyolite has erupted from the Izu–Bonin–Mariana volcanic arc (IBM arc) from its earliest stage (Eocene) to the present. Geochemically, three types of Quaternary rhyolites exist in the Izu–Bonin arc front, and they are closely related to volcano type and crustal structure. The dominantly basaltic islands of the volcanic front produce small volumes of rhyolites that we call R1. The submarine calderas of the volcanic front erupt mostly rhyolite that we call R2. Seamounts, knolls, and pillow ridges in the backarc extensional zone are mostly basaltic but also contain rhyolites that we call R3. The thickest total crust, and the thickest intermediate composition middle crust, occurs below the dominantly basaltic volcanoes, whereas the intermediate composition middle crust tends to be thinner beneath the submarine calderas. R1 rhyolites may be derived from Quaternary andesitic sources whereas R2 and R3 rhyolites may be derived from Oligocene ones. The higher CaO/Al_2O_3 in R1 compared with R2 and R3 rhyolites can be attributed to the same difference between Quaternary and Oligocene andesite sources, respectively. Light rare earth element (LREE)-depleted REE patterns of Quaternary andesites versus flat to slightly LREE-enriched patterns of Oligocene andesites are almost parallel to those of R1 and R2, respectively. Partial melts of Quaternary andesite will have low Zr/Y values such as in R1, whereas melts of Oligocene andesites will have the higher Zr/Y values of R2. Lavas from basalt-dominant volcanoes have higher Sr, Pb, and sometimes Nd isotope ratios than those from rhyolite-dominated volcanoes, which are closer to the isotope ratios of the Oligocene arc. Why and how do crustal sources differ systematically and alternately along and behind the Izu–Bonin arc? If locally developed regions within the mantle wedge (hot fingers) produce large basaltic volcanoes and remain stationary for millions of years, then basalt-dominant volcanoes eventually will overlie thicker crust. Remelting of middle crust to form rhyolite magmas takes place beneath both basaltic and rhyolitic volcanoes (R1 and R2 rhyolite, respectively). However, basalt volcanoes consume new middle crust to produce rhyolite magma whereas rhyolite volcanoes consume old Oligocene middle crust. Moreover, rhyolite volcanoes have no mantle roots beneath the crust. Instead, dikes from basalt volcanoes provide the heat source to partially melt the crust.

KEY WORDS: *arc volcano; hot fingers; middle crust; REE; rhyolite; Sr–Nd–Pb isotope*

*Corresponding author. Telephone: +81-46-867-9761. Fax: +81-46-867-9625. E-mail: tamuray@jamstec.go.jp

INTRODUCTION

The Izu–Bonin–Mariana volcanic arc (IBM arc) system is an excellent example of an intra-oceanic convergent margin where the effects of crustal anatexis and assimilation are often considered to be minimal (Stern *et al.*, 2003; Tatsumi & Stern, 2006) (Fig. 1). However, anatexis and assimilation may occur in oceanic arcs and backarcs. For example, Macpherson & Mattey (1998) suggested that low $\delta^{18}O$ intermediate melts from the Central Lau Basin resulted from assimilation of <15% of their own mass of $\delta^{18}O$-depleted oceanic crust during crystallization of a plagioclase-dominated assemblage. Assimilation of ^{18}O-poor country rock has been also proposed to explain low $\delta^{18}O$ values in lavas erupted within the Sunda arc (Harmon & Gerbe, 1992); however, the effects may be subtle isotopically and best seen in felsic melts.

Volume-weighted histograms of rock types from the Quaternary Izu–Bonin arc (30·5–35°N) suggest that dacite and/or rhyolite also form a major mode even though basalt and basaltic andesite (<57 wt % SiO_2) are clearly the predominant eruptive products (Tamura & Tatsumi, 2002). About half of the edifices at the Quaternary volcanic front are calderas dominated by rhyolite (i.e. volcanic rocks with >70 wt % SiO_2) (Yuasa & Kano, 2003). Turbidites sampled during Ocean Drilling Program (ODP) Leg 126 in the Izu–Bonin arc, which range in age from 0·1 to 31 Ma, are similarly bimodal (Gill *et al.*, 1994). Rhyolites were also abundant in the Oligocene and Eocene (Reagan *et al.*, 2008) so that the IBM oceanic arc has included abundant rhyolite from its earliest stage to the present. This is not unique to Izu. The 30–36·5°S sector of the Kermadec arc is another example of an oceanic arc with abundant Quaternary rhyolite (Smith *et al.*, 2003, 2006; Wright *et al.*, 2006). Thus, the crustal evolution of oceanic arcs must explain this bimodal volcanism of basalt and rhyolite.

In previous studies (Tamura *et al.*, 2005, 2007), we concentrated on the genesis of basalts in two of the large arc-front volcanoes, Sumisu (31·5°N, 140°E) and Torishima (30·5°N, 140·3°E), in the central Izu–Bonin arc (Fig. 2).

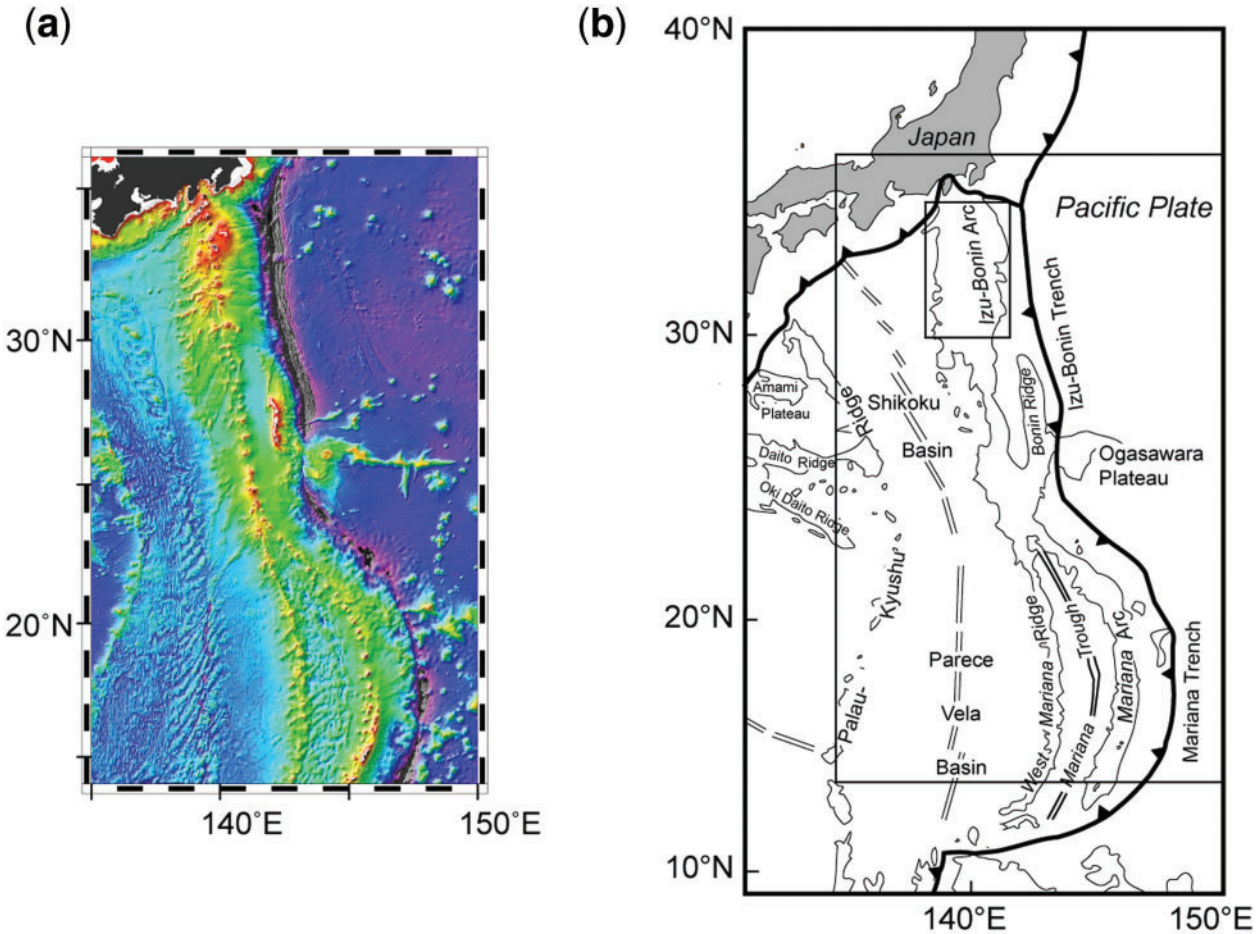

Fig. 1. (a) Topographic features of the Izu–Bonin–Mariana (IBM) arc system. (b) The structure of the IBM arc system. Double lines indicate spreading centers, active in the Mariana Trough and relic in the Shikoku and Parece Vela Basins. The Izu–Bonin, West Mariana and Mariana arcs are outlined by the 3 km bathymetric contour, and other basins and ridges are outlined by the 4 km contour (Taylor, 1992).

These volcanoes erupted low-K basalts originating from both wet and dry parental basaltic magmas (low-Zr basalts and high-Zr basalts, respectively); these parental basalts appear to result from different degrees of partial melting of the same source mantle (~20% and ~10% for wet and dry basalt magmas, respectively).

The genesis of rhyolite in oceanic arcs has been debated by a number of workers (Tamura & Tatsumi, 2002; Smith *et al.*, 2003, 2006; Shukuno *et al.*, 2006; Wright *et al.*, 2006). In this study we provide a petrological perspective on arc crustal structure and evolution by studying rhyolites from different geological settings within the Izu arc.

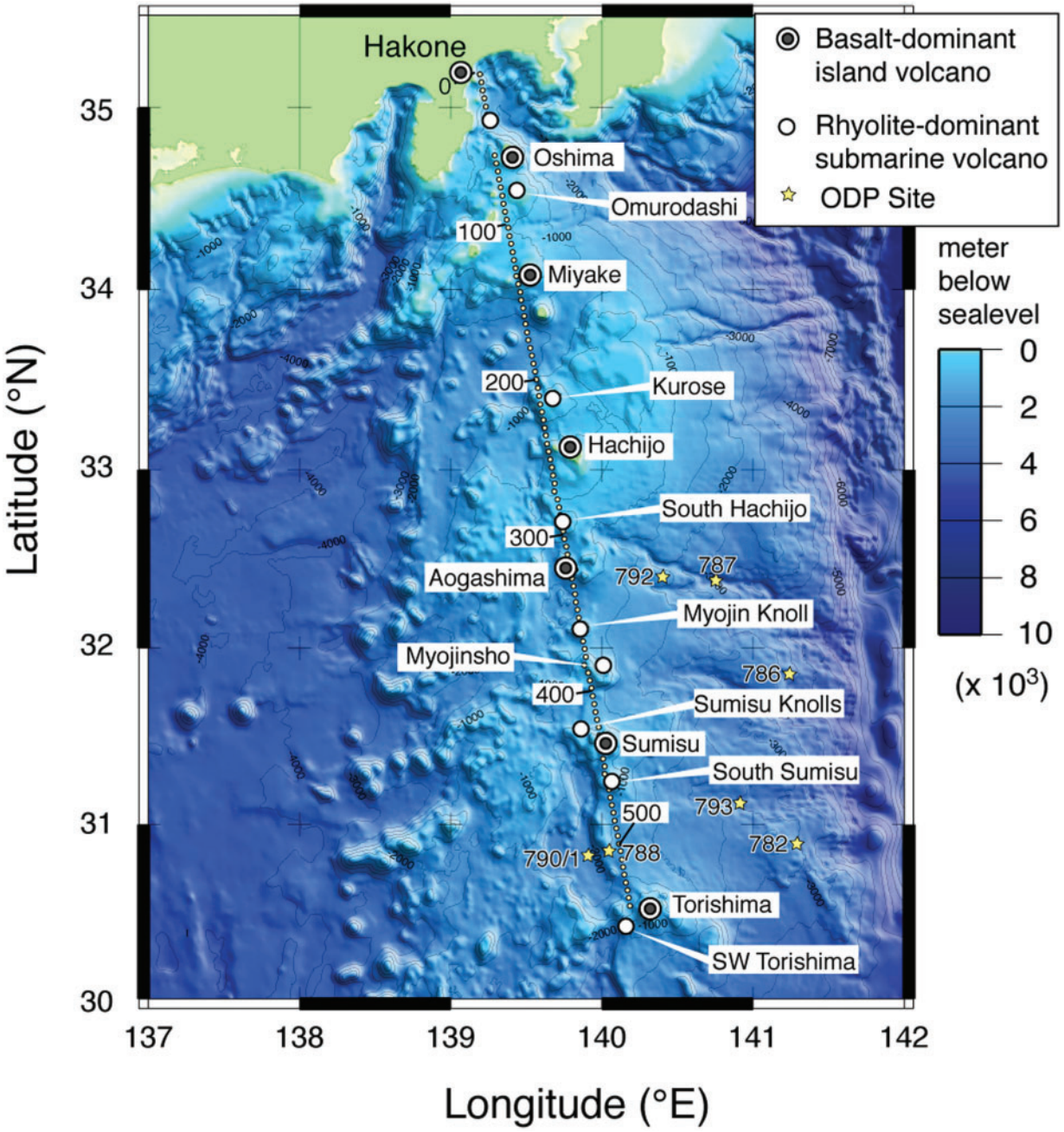

Fig. 2. Map showing the 16 Quaternary volcanoes with which this study is concerned and the location of the wide-angle seismic profile. Dots on the profile indicate the location of a total of 103 ocean bottom seismometers (OBS), which were deployed at ~5 km intervals; the numbers on the profile show the distance from its northern end (Kodaira *et al.*, 2007*a*). Numbered stars indicate sites drilled on the Philippine Sea plate in the Izu–Bonin region during ODP Legs 125 and 126.

The dominantly basaltic islands of the volcanic front produce small volumes of rhyolite that we call R1. The submarine calderas of the volcanic front erupt mostly rhyolite that we call R2. Seamounts, knolls, and pillow ridges in the backarc extensional zone are mostly basaltic but also contain rhyolites that we call R3. One or more of these rhyolite types could be melts of the crust, in which case they are probes of crustal composition, especially the middle crust, along and across the arc (Tamura & Tatsumi, 2002). Specifically, we propose that the middle crust is the source of R2 rhyolite from rhyolite-dominated calderas and that thinning of the middle crust results from its remelting caused by the intrusion of basalt dikes from nearby large basalt-dominated volcanoes (Kodaira *et al.*, 2007*a*). If so, then the remelting process might change the middle crust into denser residual lower crust. This idea also suggests that these rhyolite volcanoes have no mantle roots: no heat sources within the mantle, and no mantle-derived magmas just below the volcanoes.

This study is intended to be a progress report rather than a final interpretation of processes taking place within the Izu–Bonin arc. We attempt to reconcile the geophysical findings of Kodaira *et al.* (2007*a*, 2007*b*) with our present understanding of the petrology and volcanism, using a case study to illustrate our main points. Future work will be informed by our current interpretations and will lead to fuller understanding of intra-oceanic arc genesis.

CRUSTAL STRUCTURE AND GEOLOGICAL SETTING OF IZU RHYOLITES

The original incentive for this research was curiosity about the along-strike correlations between crustal structure and the average composition of Quaternary volcanic front magmas shown by Kodaira *et al.* (2007*a*). They conducted an active source wide-angle seismic study of the northernmost 550 km of the Izu intra-oceanic arc. Figure 2 shows the location of their seismic profile. A total of 103 ocean bottom seismometers (OBS) were deployed at ~5 km intervals along the profile. Figure 2 also shows the location of the basalt-dominant island volcanoes and rhyolite-dominant submarine calderas. Figure 3a shows the average SiO_2 content (wt %) of Quaternary volcanic rocks and the thickness of the middle crust along the profile of Fig. 2 based on Kodaira *et al.* (2007*a*) and additional data from this study. Kodaira *et al.* (2007*a*) showed (1) a remarkable along-arc periodic variation with a wavelength of 80–100 km in average crustal velocities and the thickness of felsic to intermediate composition middle crust with a P-wave velocity (V_p) of 6·0–6·8 km/s, and (2) that these structural variations correlate well with the average chemical compositions of the overlying arc volcanoes. That is, the thickest total crust, and the thickest intermediate composition middle crust, occurs predominantly below the basaltic volcanoes, whereas the intermediate composition middle crust tends to be thinner beneath the dacitic to rhyolitic volcanoes.

Figure 3b shows the schematic relationship between the volcanoes and crustal structure along the Izu–Bonin volcanic front based on Kodaira *et al.* (2007*a*) and Fig. 3a. It is remarkable that the velocity structure of this part of the Izu–Bonin arc crust, which has a complex 50 Myr history, correlates with the chemical composition of the Quaternary volcanoes. Moreover, why should basaltic volcanoes overlie lower average velocity (more continental-like) crust compared with the silicic volcanoes, and why should rhyolitic volcanoes overlie thinner middle crust?

ANALYTICAL METHODS

We present new analyses of rhyolites and summarize others from a new database for IBM volcanic rocks called GANSEKI (http://www.jamstec.go.jp/ganseki/index.html), which includes previously unpublished X-ray fluorescence (XRF) major and trace element analyses of samples collected by JAMSTEC. The following analytical methods apply to both.

After initial splitting and jaw crushing, all samples were pulverized in an agate ball mill. Major and trace elements were determined by XRF at IFREE, JAMSTEC. Trace elements were analyzed on pressed powder discs, and major elements were determined on fused glass discs. A mixture of ~0·4 g of each powdered sample and 4 g of anhydrous lithium tetraborate ($Li_2B_4O_7$) was used; no matrix correction was applied because of the high dilution involved. All discussion in this paper refers to analyses that have been normalized to 100% on a volatile-free basis with total iron calculated as FeO.

For the samples reported here, additional trace elements were analyzed by inductively coupled plasma mass spectrometry (ICP-MS) using an Agilent 7500ce system (Agilent Technologies, Tokyo Japan) fitted with PFA sample introducing and a Pt-inject torch system. The ICP-MS system was operated at no collision gas and multi-tune acquisition mode. This combination of the system allowed a wide range of elements to be precisely determined using a pulse counting detector, and also hydrofluoric acid containing sample solution to be delivered directly into the plasma. Sample dissolution, preparation and measurement were as described by Chang *et al.* (2003). Accurately weighed 100 mg aliquots of powdered samples were digested in screw-cap PFA vials with mixed acids (0·65 ml $HClO_4$ and 2 ml HF) on a hot plate at 130–140°C for 3 days. After drying, 1 ml $HClO_4$ was added, and the vials were heated at 160°C overnight. They were then opened to evaporate the solutions at a gradually increased temperature of up to 190°C to drive off excess HF and convert the

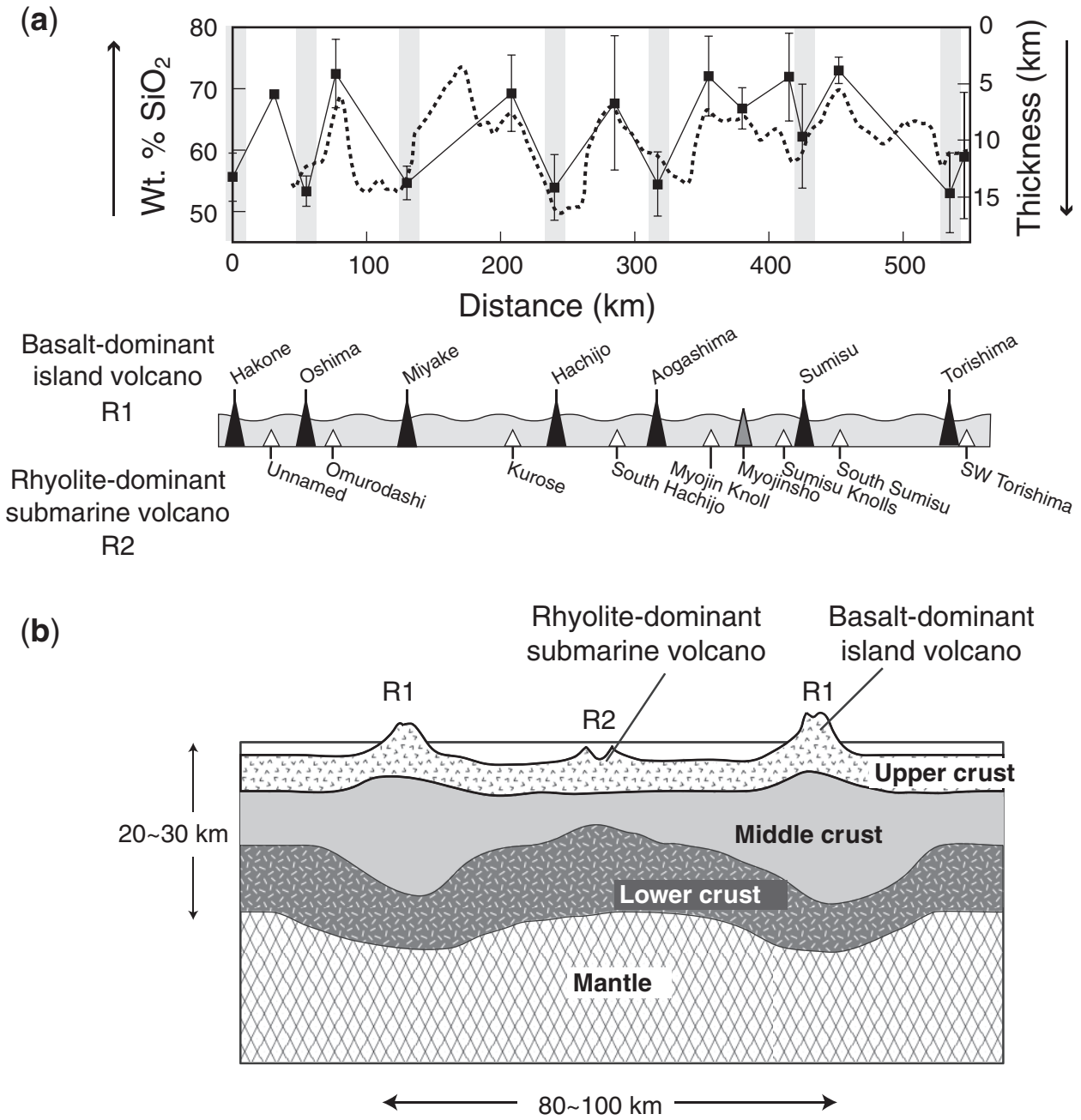

Fig. 3. (a) Along-arc crustal structure (dotted line; thickness of middle crust with V_p of 6·0–6·8 km/s at depths between 5 and 20 km) and average wt % SiO_2 of volcanic rocks ({■}) sampled and dredged from the 16 Quaternary volcanoes of the Izu–Bonin arc shown in Fig. 2. The basalt-dominant island volcanoes produce small volumes of rhyolites that we call R1. The rhyolite-dominant submarine volcanoes erupt mostly rhyolite that we call R2. (b) Schematic crustal structure of the Izu–Bonin arc volcanic front showing alternating basalt-dominant island volcanoes and rhyolite-dominant submarine volcanoes, which have thick and thin middle crust and erupt R1 and R2 rhyolite, respectively.

fluoride into chlorides. The residues were taken into 2 ml 6 mol/l HNO_3, moderately heated and then evaporated at 120°C to incipient dryness. The final dissolution was performed with 10 ml 2% HNO_3. Prior to analysis, In and Bi were added to aliquots of sample solutions as internal standards to correct for drift during measurements. Measured Eu and Gd concentrations were corrected for oxide and hydroxide interferences. The analytical results of repeated analyses of well-established reference standards (JB-2 and BHVO-1) agreed very well with recommended

values, demonstrating that the rare earth elements (REE) and trace element determinations had high accuracy and reproducibility.

Sr, Nd and Pb isotope analyses were conducted both at IFREE, JAMSTEC and the University of California, Santa Cruz. The analytical procedure used at IFREE for chemical separation and mass spectrometry for Sr, Nd and Pb isotope determinations has been outlined by Miyazaki *et al.* (2007). Total procedural blanks for Sr, Nd and Pb during the measurement period were less than 15 pg, 3 pg and 6 pg, respectively. Mass spectrometry was performed on a Thermo-Finnigan® Triton TI. Lead isotope ratios were measured using the double spike method. Measured isotopic ratios for standard materials were $^{87}Sr/^{86}Sr = 0{\cdot}710258 \pm 07$ (2σ) for NIST 987 ($n = 5$), $^{143}Nd/^{144}Nd = 0{\cdot}512097 \pm 17$ (2σ), for JNdi-1 ($n = 8$), and $^{208}Pb/^{204}Pb = 36{\cdot}7136 \pm 86$ (2σ), $^{207}Pb/^{204}Pb = 15{\cdot}4947 \pm 34$ (2σ) and $^{206}Pb/^{204}Pb = 16{\cdot}9351 \pm 38$ (2σ) for NIST 981 ($n = 5$). Analytical methods used at UCSC for isotope ratios have been summarized by Ryder *et al.* (2006). Results are normalized to the same values as listed above. Hf isotope ratios were measured following the methods of Ryder *et al.* (2006) and are normalized to $^{176}Hf/^{177}Hf = 0{\cdot}282160$ for JMC 475.

Electron-microprobe analyses were carried out using the JAMSTEC JEOL JXA-8900 Superprobe equipped with five wavelength-dispersive spectrometers (WDS). Pyroxene and plagioclase analyses were made with a counting time of 20 s, using an accelerating voltage of 15 kV and a beam current of 15 nA.

Representative major and trace element and Sr–Nd–Pb–Hf isotope data for silicic rocks from the Izu–Bonin arc are reported in Table 1. The entire XRF dataset is available as an Electronic Appendix, which may be downloaded from http://www.petrology.oxfordjournals.org/.

THREE TYPES OF RHYOLITE IN NORTH IZU

A total of 236 chemical analyses of silicic magmas (>66 wt % SiO_2) from 16 Quaternary arc front volcanoes and four locations in the backarc (Aogashima Rift, Myojin Rift, Sumisu Rift and Torishima Rift) were compiled for this study. Based on the chemical analyses of all volcanic rocks and sediments from north Izu, we estimate that about one-third of the Quaternary magmatism by mass has been felsic (Gill *et al.*, 1994; Tamura & Tatsumi, 2002). The rhyolites are of three kinds. Most are low-K, although some R2 and R3 rhyolites are medium-K according to the classification scheme of Gill (1981). They show a complete chemical gradation from the tholeiitic to the calc-alkaline field of Miyashiro (1974), but the R2 and R3 rhyolites have relatively higher and lower Mg-number values [100Mg/(Mg + ΣFe)], respectively, than the R1 rhyolites.

R1 rhyolites are from basalt-dominant island volcanoes, which are the largest edifices. Labeled islands in Fig. 2 are the summits of these volcanoes. For example, the main edifice of Torishima volcano rises from an ocean depth of ~1000 m and is about 20 km in diameter; Torishima island lies along the south rim of a submarine caldera (Tamura *et al.*, 2007). The Oshima and Miyake volcanoes with volumes of 415 and 519 km^3, respectively, are the largest (Suga & Fujioka, 1990).

R2 rhyolites are from entirely rhyolite-dominant submarine calderas. Omurodashi, Kurose, Myojin Knoll and South Sumisu have volumes of 125, 139, 106 and 100 km^3, respectively (Suga & Fujioka, 1990). In a subsequent section we include a detailed discussion of two examples of this type, South Sumisu and SW Torishima. Myojinsho (326 km^3) is a large dacite-dominant submarine volcano and is the one anomaly in our generalization. It has R1 geochemistry (which is how we plot it) despite its felsic character. Sumisu shows bimodal magmatism (Tamura *et al.*, 2005; Shukuno *et al.*, 2006) and its rhyolites are similar to those from the basalt-dominant volcanoes.

R3 rhyolites are from backarc rifts and knolls. Between 29° and 33°N several narrow grabens, a few tens of kilometers wide, lie just behind the volcanic front. The Sumisu Rift is one of them, and is the best-studied present-day example of rhyolite erupted during the initial stages of back-arc basin evolution (Ikeda & Yuasa, 1989; Fryer *et al.*, 1990; Hochstaedter *et al.*, 1990*a*, 1990*b*; Gill *et al.*, 1992). We present new data for 19 additional rhyolites from the Aogashima, Myojin, Sumisu and Torishima Rifts. Rhyolite pumice or lava also was recovered in about half of the 120 dredges from throughout the 100 km wide Izu backarc by Hochstaedter *et al.* (2000). Of the 17 that were analyzed, 15 are R3 in composition. In contrast, all rhyolite pumice in ODP cores in the Izu forearc—even from near rhyolite-dominated volcanoes—is R1 (Gill *et al.*, 1992). We interpret this contrast to mean that the ubiquitous rhyolites in the backarc are locally derived and not rafted in from the volcanic front. If so, then R3 is potentially widespread and very common in the backarc. There is a significant across-arc chemical variation in Zr, Nb, and K concentrations and Sr, Nd and Pb isotope ratios across the backarc that may extend to the rhyolites (Hochstaedter *et al.*, 2000, 2001; Ishizuka *et al.*, 2003*a*). In this study, however, we will discuss only the relationships between rhyolite composition and crustal structure near the Izu–Bonin volcanic front.

Figure 4a shows silica variation diagrams for major elements (TiO_2, Al_2O_3, FeO*, MgO, CaO, Na_2O and K_2O) and Mg value, and FeO* diagrams for TiO_2, Al_2O_3, CaO and K_2O. Figure 4b shows the variation of selected trace elements (Ba, Sr, Rb, Zr and Y with SiO_2). R1 rhyolites extend to the lowest SiO_2 and highest FeO* contents and are lower in Al_2O_3 and K_2O but higher in CaO than the others at any silica content. R1 rhyolites also have lower

Table 1: Major and trace element and Sr–Nd–Pb–Hf isotopic data for representative rhyolites from the Izu–Bonin arc

Cruise:	KR02-16				NT02-10		
Locality:	Torishima				Sumisu		
Sample:	D9-R03	D19-R03	D21-R01	D21- pumice2	3K572- R3	3K574-R6	3K576-R1
Latitude (°N):	30·53	30·46	30·58	30·58	31·463	31·478	31·507
Longitude (°E):	140·334	140·391	140·334	140·334	140·078	140·014	140·093
Rhyolite type:	R1	R1	R1	R1	R1	R1	R1
Rock type:	pumice	lava	lava	pumice	lava	lava	pumice
SiO_2	73·12	67·96	67·59	72·12	69·44	66·41	71·12
TiO_2	0·48	0·59	0·76	0·47	0·66	0·73	0·46
Al_2O_3	12·90	13·71	14·75	13·63	13·99	14·57	12·66
Fe_2O_3	3·37	5·98	6·09	4·11	5·67	6·88	4·97
MnO	0·15	0·16	0·17	0·15	0·19	0·18	0·15
MgO	0·58	1·04	1·34	1·31	0·92	1·32	0·40
CaO	2·69	4·11	5·05	3·27	4·02	4·98	2·93
Na_2O	4·50	4·26	4·11	4·42	4·21	4·11	4·39
K_2O	0·81	0·70	0·58	0·78	0·72	0·73	0·88
P_2O_5	0·10	0·16	0·17	0·11	0·18	0·20	0·10
Total	98·71	98·67	100·60	100·37	99·99	100·10	98·07
Mg-no.	25·45	25·65	30·31	38·49	24·27	27·48	13·86
CaO/Al_2O_3	0·21	0·30	0·34	0·24	0·29	0·34	0·23
Trace elements (ppm) by XRF							
Ba	179·5	141·5	137·0	167·8	200·6	175·8	224·7
Ni	8·3	7·0	8·2	1·1	7·8	9·0	8·4
Cu	3·9	36·4	3·6	26·4	1·8	12·0	15·3
Zn	88·1	96·3	99·4	101·4	99·4	101·0	101·9
Pb	5·4	5·0	6·1	6·2	5·0	4·2	4·7
Th	0·9		1·2	1·0		1·4	1·0
Rb	10·5	9·1	5·2	10·8	11·1	10·7	13·2
Sr	152·6	165·2	201·1	157·6	184·5	189·2	143·3
Y	42·3	40·6	37·7	41·7	43·0	39·6	49·3
Zr	103·0	85·3	82·3	99·9	101·3	96·8	127·0
Nb	1·1	0·7	1·0	1·1	1·0	1·2	1·0
Zr/Y	2·43	2·10	2·18	2·40	2·36	2·44	2·58
Trace elements (ppm) by ICP-MS							
Sc		15·6	13·6	15·8			
V							
Cr							
Co		3·96	3·91	3·48			
Ni		5·12	39·6	5·63			
Cu							
Rb		9·34	6·86	9·23			
Sr		153	113	142			
Y		42·7	36·5	44·2			
Zr		86·7	99·4	97·2			
Nb		0·799	1·05	0·927			
Cs		0·980	0·755	1·07			
Ba		151	124	166			
La	4·55	4·22	4·17	4·50	4·24	4·26	5·05
Ce	12·6	11·5	14·1	12·7	12·1	12·1	14·4
Pr	2·20	2·08	2·05	2·20	2·08	2·04	2·42
Nd	11·8	10·9	10·5	11·4	11·8	11·4	12·9
Sm	3·92	3·76	3·62	3·91	4·02	3·84	4·39
Eu	1·15	1·11	1·12	1·13	1·29	1·25	1·18
Gd	5·31	4·91	4·77	5·20	5·96	5·61	5·91
Tb	0·956	0·913	0·908	0·973	1·04	0·958	1·06
Dy	6·47	6·21	5·86	6·46	7·05	6·51	7·28
Ho	1·44	1·44	1·33	1·50	1·55	1·43	1·6
Er	4·43	4·15	3·80	4·26	4·74	4·36	4·9
Tm	0·671	0·645	0·593	0·682	0·687	0·629	0·726
Yb	4·53	4·24	3·97	4·49	4·65	4·18	4·92
Lu	0·709	0·655	0·587	0·674	0·707	0·649	0·759
Hf		2·67	3·22	2·98			
Ta		0·068	0·088	0·075			
Tl							
Pb	4·82	5·15	6·23	5·48	4·25	4·18	4·43
Th	0·449	0·439	0·581	0·496	0·541	0·589	0·642
U	0·381	0·370	0·397	0·400	0·332	0·347	0·412
$^{87}Sr/^{86}Sr$	0·703723	0·703722	0·703694	0·703791	0·703682		
$^{143}Nd/^{144}Nd$	0·513120	0·513116	0·513123	0·513123	0·513098		
$^{206}Pb/^{204}Pb$	18·4730	18·4623	18·4702	18·4726	18·5402		
$^{207}Pb/^{204}Pb$	15·5505	15·5487	15·5482	15·5518	15·5476		
$^{208}Pb/^{204}Pb$	38·3410	38·324	38·3334	38·3439	38·418		
$^{176}Hf/^{177}Hf$	0·283272	0·283270	0·283268	0·283275	0·283232		

Table 1: Continued

Cruise:	NT02-10		Y96-3	Y96-3	NT06-21		
Locality:	Sumisu		Aogashima	Hachijo	SW Torishima		
Sample:	3K576-R6	3K576-R7	9102	05110502B	HD-616- R04	HD-616- R10	HD-616- R14
Latitude (°N):	31·51	31·51	32·5	33·133	30·407	30·411	30·414
Longitude (°E):	140·087	140·085	139·706	139·769	140·095	140·111	140·124
Rhyolite type:	R1	R1	R1	R1	R2	R2	R2
Rock type:	lava	lava	lava	pumice	lava	lava	lava
SiO_2	69·78	72·43	68·02	66·38	69·04	70·19	70·28
TiO_2	0·68	0·42	0·55	0·71	0·74	0·58	0·57
Al_2O_3	14·27	12·71	14·45	15·49	14·05	14·66	14·50
Fe_2O_3	5·06	4·75	6·63	6·27	5·55	4·17	3·98
MnO	0·16	0·15	0·19	0·20	0·19	0·16	0·16
MgO	1·00	0·40	0·74	1·60	1·07	0·91	0·85
CaO	3·83	2·85	4·23	5·36	4·09	3·58	3·42
Na_2O	4·69	4·51	4·33	3·93	4·25	4·68	4·63
K_2O	0·76	0·91	0·60	0·45	0·90	0·97	1·13
P_2O_5	0·17	0·09	0·12	0·18	0·17	0·14	0·14
Total	100·40	99·22	99·86	100·57	100·05	100·03	99·66
Mg-no.	28·18	14·15	18·14	33·35	27·55	30·14	29·74
CaO/Al_2O_3	0·27	0·22	0·29	0·35	0·29	0·24	0·24
Trace elements (ppm) by XRF							
Ba	192·2	225·3	121·3	229·0	120·9	133·7	133·5
Ni	5·7	6·8	8·8		2·2	2·6	2·6
Cu	5·8	10·9			4·5	3·1	3·1
Zn	89·5	99·5			97·8	84·0	79·5
Pb	3·9	5·0	2·8		3·3	4·1	3·1
Th	0·6	0·7	1·5		1·3	1·5	1·6
Rb	6·8	13·6	6·3	10·2	12·1	14·9	15·2
Sr	168·3	141·6	177·9	150·3	187·5	184·1	180·5
Y	40·4	50·1	39·4	55·6	33·7	29·1	29·2
Zr	112·2	131·6	96·5	122·2	116·0	126·5	130·7
Nb	0·8	1·0	0·4	0·9	1·5	1·7	2·0
Zr/Y	2·78	2·63	2·45	2·20	3·44	4·35	4·48
Trace elements (ppm) by ICP-MS							
Sc					18·0	12·9	12·8
V							
Cr							
Co					19·0	12·9	11·6
Ni					1·00	1·02	1·00
Cu					5·11	4·42	3·95
Rb					10·4	13·3	13·5
Sr					175	173	169
Y					32·2	27·4	27·6
Zr					112	121	126
Nb					1·62	1·75	1·80
Cs					0·441	0·471	0·482
Ba					118	133	136
La	4·36	5·95		4·84	6·55	6·92	7·13
Ce	12·4	17		14·3	16·5	16·9	17·4
Pr	2·08	2·89		2·34	2·56	2·52	2·58
Nd	11·5	15·4		13·5	12·7	11·9	12·1
Sm	3·88	5·15		4·90	3·83	3·39	3·40
Eu	1·23	1·38		1·37	1·28	1·12	1·10
Gd	5·65	6·95		6·25	4·94	4·19	4·22
Tb	0·983	1·26		1·15	0·876	0·738	0·742
Dy	6·71	8·64		8·44	5·80	4·82	4·86
Ho	1·47	1·9		1·81	1·26	1·06	1·06
Er	4·53	5·82		5·30	3·88	3·25	3·29
Tm	0·66	0·869		0·877	0·575	0·490	0·493
Yb	4·43	5·85		5·47	3·92	3·38	3·41
Lu	0·681	0·907		0·843	0·611	0·538	0·543
Hf				3·54	3·27	3·38	3·47
Ta					0·154	0·168	0·171
Tl					0·070	0·095	0·096
Pb	3·96	5·18		4·23	2·76	2·80	2·76
Th	0·635	0·781		0·441	0·819	0·906	0·922
U	0·392	0·486		0·317	0·503	0·446	0·433
$^{87}Sr/^{86}Sr$		0·703777			0·703367	0·703274	0·703270
± 2SE					6	5	7
$^{143}Nd/^{144}Nd$		0·513101			0·513093	0·513104	0·513084
± 2SE					11	12	13
$^{206}Pb/^{204}Pb$		18·5087			18·3916	18·3604	18·3594
± 2SE					24	4	7
$^{207}Pb/^{204}Pb$		15·5401			15·5306	15·5275	15·5268
± 2SE					21	4	6
$^{208}Pb/^{204}Pb$		38·3809			38·2065	38·1754	38·1700
± 2SE					51	10	16
$^{176}Hf/^{177}Hf$		0·283246					

Table 1: Continued

Cruise:	NT06-21	KR04-04	NT06-21			KR02-16	NT04-10
Locality:	SW Torishima	South Sumisu	South Sumisu			Sumisu Knoll No. 1	Kaiyo Knoll
Sample:	HD-616-R16	DR06-R01	HD-617-R01	HD-617-R02	HD-617-R08	D6-R5	H341-R01
Latitude (°N):	30·415	31·154	31·259	31·259	31·258	31·535	31·498
Longitude (°E):	140·126	140·018	139·947	139·948	139·951	139·854	139·787
Rhyolite type:	R2	R2	R2	R2	R2	R2	R2
Rock type:	lava	lava	lava	lava	lava	pumice	pumice
SiO_2	70·02	71·24	71·72	71·91	71·45	75·58	75·46
TiO_2	0·69	0·36	0·59	0·64	0·58	0·30	0·30
Al_2O_3	14·01	14·81	13·73	13·27	13·55	12·93	13·00
Fe_2O_3	4·95	3·77	3·94	4·30	4·23	2·15	2·20
MnO	0·18	0·18	0·11	0·14	0·09	0·11	0·11
MgO	0·94	0·61	0·88	0·85	1·14	0·26	0·29
CaO	3·75	2·91	3·38	3·23	3·27	1·86	1·89
Na_2O	4·38	5·14	4·46	4·42	4·52	4·99	5·10
K_2O	1·03	0·94	0·86	1·03	0·81	1·18	1·19
P_2O_5	0·17	0·10	0·12	0·13	0·12	0·06	0·06
Total	100·11	100·05	99·77	99·92	99·74	99·40	99·60
Mg-no.	27·27	24·23	30·66	28·15	34·75	19·30	20·90
CaO/Al_2O_3	0·27	0·20	0·25	0·24	0·24	0·14	0·15
Trace elements (ppm) by XRF							
Ba	131·6	164·0	155·2	151·0	156·7	215·1	207·4
Ni	2·2		3·2	2·4	2·4	8·8	
Cu		1·7	7·9	4·7	4·8		3·0
Zn	91·6	92·7	66·3	74·0	69·4	64·7	59·8
Pb	4·4	4·5	4·7	4·8	3·9	4·6	5·0
Th	1·0	1·1	1·1	1·4	0·5	1·0	1·0
Rb	13·5	13·7	11·4	14·5	11·1	20·6	21·4
Sr	180·6	208·3	158·6	152·7	158·1	129·6	128·6
Y	33·1	39·7	38·1	39·2	37·9	45·6	44·9
Zr	123·4	153·8	129·4	130·7	128·6	200·9	198·1
Nb	1·8	1·8	1·2	1·2	1·2	2·0	2·0
Zr/Y	3·73	3·87	3·40	3·33	3·39	4·41	4·42
Trace elements (ppm) by ICP-MS							
Sc	16·3		15·6	16·7	15·6		
V							
Cr							
Co	13·7		14·0	15·2	15·5		
Ni	0·81		1·18	1·25	1·71		
Cu	2·72		8·41	5·59	5·90		
Rb	12·0		10·3	12·0	9·40		
Sr	169		149	143	146		
Y	31·5		35·8	37·1	36·0		
Zr	121		125	127	126		
Nb	1·73		1·27	1·29	1·26		
Cs	0·48		0·145	0·573	0·210		
Ba	129		154	159	150		
La	6·94	9·20	6·50	6·62	6·57	6·83	
Ce	17·3	24·5	17·3	17·5	17·3	18·1	
Pr	2·63	3·47	2·74	2·78	2·76	2·77	
Nd	12·9	16·6	13·7	14·1	13·7	13·2	
Sm	3·83	4·97	4·18	4·31	4·19	3·72	
Eu	1·25	1·50	1·19	1·21	1·18	0·929	
Gd	4·86	5·88	5·35	5·50	5·36	4·44	
Tb	0·858	1·02	0·956	0·983	0·953	0·782	
Dy	5·65	6·54	6·32	6·52	6·35	5·29	
Ho	1·23	1·48	1·38	1·42	1·40	1·16	
Er	3·79	4·42	4·26	4·36	4·32	3·57	
Tm	0·564	0·693	0·634	0·651	0·644	0·537	
Yb	3·84	4·39	4·31	4·44	4·38	3·69	
Lu	0·605	0·711	0·671	0·694	0·686	0·572	
Hf	3·45	4·24	3·91	3·97	3·90		
Ta	0·16	0·179	0·131	0·131	0·129		
Tl	0·081		0·047	0·103	0·030		
Pb	2·88	4·01	3·29	4·22	2·96	2·87	
Th	0·885	1·09	0·832	0·847	0·827	0·976	
U	0·425	0·449	1·06	0·491	0·534	0·424	
$^{87}Sr/^{86}Sr$	0·7033467		0·7034217	0·7034216	0·7034316		
± 2SE	7		7	6	6		
$^{143}Nd/^{144}Nd$	0·513080		0·513091	0·513072	0·513057		
± 2SE	12		8	12	11		
$^{206}Pb/^{204}Pb$	18·3819		18·3701	18·3837	18·3612		
± 2SE	15		28	24	30		
$^{207}Pb/^{204}Pb$	15·5308		15·5208	15·5334	15·5148		
± 2SE	13		25	21	26		
$^{208}Pb/^{204}Pb$	38·2030		38·1892	38·2255	38·1740		
± 2SE	33		66	53	68		
$^{176}Hf/^{177}Hf$							

Table 1: Continued

Cruise:	KR02-16	N91-05	N96-11	NT99-09	NT98-10	N84-8404	N92-05
Locality:	Kaiyo Knoll	Myojin Knoll	Myojin Knoll	Minami Hachijo	Minami Hachijo	Sagami Bay	Sumisu Rift
Sample:	D7-R1	2K-555-R1	2K-892-R3	2K-1109-R2-1	2K-1046-R3-2	2K-118-R1	2K-623-R1
Latitude (°N):	31·514	32·1	32·117	32·7	32·7	34·9	31·367
Longitude (°E):	139·814	139·833	139·833	139·75	139·75	139·217	139·833
Rhyolite type:	R2	R2	R2	R2	R2	R2	R3
Rock type:	pumice	lava	lava	lava	pumice	lava	pumice
SiO_2	75·62	72·80	71·89	72·83	70·47	69·09	73·75
TiO_2	0·30	0·36	0·42	0·27	0·49	0·47	0·24
Al_2O_3	12·87	14·08	13·73	13·34	14·59	14·95	13·14
Fe_2O_3	2·09	3·10	4·06	2·16	3·46	4·78	2·53
MnO	0·10	0·11	0·14	0·07	0·16	0·13	0·14
MgO	0·26	0·65	0·90	0·42	0·80	1·45	0·22
CaO	1·84	3·17	3·50	2·42	2·91	4·68	1·72
Na_2O	4·94	4·63	4·43	4·47	5·22	3·75	5·31
K_2O	1·16	0·75	0·64	1·29	1·11	1·07	1·22
P_2O_5	0·06	0·09	0·10	0·06	0·12	0·09	0·06
Total	99·23	99·74	99·80	97·34	99·32	100·46	98·32
Mg-no.	19·54	29·30	30·49	27·99	31·32	37·58	14·80
CaO/Al_2O_3	0·14	0·23	0·25	0·18	0·20	0·31	0·13
Trace elements (ppm) by XRF							
Ba	196·4	157·0	144·6	188·1	181·1	320·9	173·3
Ni	10·3	2·8	2·7	3·6	6·8	2·6	2·3
Cu		4·6	6·5	7·5	6·4	16·3	
Zn	64·4	56·0	77·4	68·0	91·0	45·6	80·0
Pb	3·1	4·3	4·0	5·4	5·3	5·3	4·6
Th	1·7	0·7	1·0	1·2	2·1	1·6	1·3
Rb	20·6	11·0	9·0	15·0	19·7	18·8	23·7
Sr	128·5	144·9	146·7	161·8	181·6	190·4	115·3
Y	45·2	32·7	38·4	47·7	44·9	23·5	52·0
Zr	200·5	135·6	124·6	195·5	217·0	111·0	216·6
Nb	2·1	1·2	1·1	2·7	3·8	1·0	2·7
Zr/Y	4·43	4·15	3·24	4·10	4·83	4·72	4·17
Trace elements (ppm) by ICP-MS							
Sc		11·3	15·4	10·4	12·2		
V							
Cr							
Co		16·2	21·7	12·0	15·4		
Ni		1·25	2·19	1·65	5·26		
Cu		5·48	6·10	4·93	6·42		
Rb		9·71	7·76	13·1	17·3		
Sr		134	134	143	165		
Y		30·3	36·1	43·1	42·7		
Zr		127	119	159	205		
Nb		1·18	1·22	2·72	4·16		
Cs		0·681	0·545	0·574	0·599		
Ba		164	141	181	181		
La		5·45	5·10	9·06	11·6		
Ce		15·0	14·8	24·6	29·7		
Pr		2·33	2·43	3·63	4·28		
Nd		11·5	12·6	17·2	20·0		
Sm		3·41	3·99	5·07	5·47		
Eu		0·991	1·20	1·12	1·50		
Gd		4·34	5·25	6·18	6·43		
Tb		0·777	0·945	1·13	1·14		
Dy		5·17	6·34	7·51	7·42		
Ho		1·14	1·39	1·64	1·61		
Er		3·57	4·28	5·11	4·97		
Tm		0·540	0·641	0·777	0·746		
Yb		3·74	4·34	5·32	5·08		
Lu		0·592	0·678	0·825	0·791		
Hf		3·75	3·60	4·89	5·55		
Ta		0·129	0·126	0·249	0·337		
Tl		0·111	0·102	0·098	0·121		
Pb		3·44	4·12	4·68	4·21		
Th		0·578	0·482	1·03	1·49		
U		0·326	0·432	0·705	0·596		
$^{87}Sr/^{86}Sr$		0·703414	0·703410	0·703323	0·703249		
± 2SE		6	6	7	7		
$^{143}Nd/^{144}Nd$		0·513057	0·513066	0·513060	0·513055		
± 2SE		11	12	10	11		
$^{206}Pb/^{204}Pb$		18·4236	18·4365	18·3130	18·2402		
± 2SE		16	18	22	11		
$^{207}Pb/^{204}Pb$		15·5272	15·5478	15·5222	15·5057		
± 2SE		14	16	21	10		
$^{208}Pb/^{204}Pb$		38·3309	38·3765	38·2168	38·1100		
± 2SE		34	39	53	29		
$^{176}Hf/^{177}Hf$							

Table 1: Continued

Cruise:	N92-05	NT04-10					Ref.
Locality:	Sumisu Rift	Knoll 336		Myojin Rift		Aogashima Rift	standard
Sample:	2K-623-R3	H336-R02	H336-R07	D624-3	51-1	48-4	JR-1
Latitude (°N):	31·367	32·514	31·516	31·57	31·92	32·16	value
Longitude (°E):	139·833	139·673	139·674	139·62	139·62	139·725	
Rhyolite type:	R3	R3	R3	R3	R3	R3	
Rock type:	pumice	lava	pumice	lava	lava	lava	
SiO_2	74·10	74·77	76·07	75·65	75·72	72·82	
TiO_2	0·38	0·28	0·33	0·18	0·34	0·42	
Al_2O_3	13·78	12·86	13·18	12·83	13·42	13·77	
Fe_2O_3	2·40	1·95	2·03	2·67	2·47	3·30	
MnO	0·13	0·08	0·10	0·15	0·16	0·11	
MgO	0·50	0·36	0·33	0·15	0·48	0·72	
CaO	2·15	2·04	2·03	1·27	2·02	3·19	
Na_2O	5·31	4·29	4·89	5·71	5·36	4·78	
K_2O	1·01	1·86	1·23	1·47	1·03	0·77	
P_2O_5	0·08	0·06	0·06	0·02	0·05	0·11	
Total	99·83	98·54	100·25	100·10	101·10	99·99	
Mg-no.	29·33	26·87	24·60	10·02	27·85	29·88	
CaO/Al_2O_3	0·16	0·16	0·15	0·10	0·15	0·23	
Trace elements (ppm) by XRF							
Ba	153·9	199·3	193·6				
Ni	4·2			10·8			
Cu	1·7	2·0	2·5				
Zn	66·7	33·6	42·8				
Pb	3·8	4·4	4·6				
Th	2·1	1·1	1·3				
Rb	13·5	32·2	19·0	21·9		11·2	
Sr	142·4	119·0	131·0	81·5		136·1	
Y	46·2	27·0	30·7	62·9		36·4	
Zr	220·5	155·7	170·0	269·6		146·2	
Nb	2·5	2·3	2·4				
Zr/Y	4·77	5·77	5·55	4·29		4·01	
Trace elements (ppm) by ICP-MS							
Sc		5·9	8·1	10·6	14·1		4·84
V		18·6	30·9	20·5	10·2		
Cr		7·83	10·1	4·67	5·94		
Co		1·87	5·30	1·45	1·76		
Ni		0·83	7·98	8·43	2·10		
Cu							
Rb		22·4	15·3	21·0	13·2		245
Sr		106	124	78·8	135		27·3
Y		29·1	31·9	62·1	53·2		38·3
Zr		144	163	217	162		91·0
Nb		2·40	2·60	5·04	2·93		14·0
Cs		1·07	0·450	0·731	0·776		19·8
Ba		184	184	165	167		45·1
La		9·82	10·1	15·5	10·4		18·9
Ce		23·0	24·2	40·6	27·6		45·4
Pr		3·17	3·38	6·16	4·43		5·75
Nd		13·0	14·2	27·7	21·2		22·7
Sm		3·19	3·50	7·46	5·84		5·67
Eu		0·687	0·838	1·46	1·63		0·254
Gd		3·56	3·99	8·10	6·88		5·60
Tb		0·631	0·719	1·45	1·23		0·971
Dy		4·13	4·51	9·33	7·92		6·14
Ho		0·926	1·02	2·09	1·75		1·28
Er		2·78	3·09	6·17	5·12		4·07
Tm		0·457	0·488	0·963	0·799		0·627
Yb		3·11	3·32	6·30	5·06		4·55
Lu		0·491	0·519	0·962	0·766		0·692
Hf		3·55	3·79	5·50	4·17		4·66
Ta		0·232	0·245	0·385	0·218		1·53
Tl							1·52
Pb		3·77	4·54	3·82	4·44		18·4
Th		1·41	1·30	1·68	1·10		25·3
U		0·571	0·529	0·596	0·406		8·56
$^{87}Sr/^{86}Sr$		0·703099	0·703274		0·702911		
$^{143}Nd/^{144}Nd$		0·513097	0·513103		0·513090		
$^{206}Pb/^{204}Pb$		18·3075	18·3033		18·2864		
$^{207}Pb/^{204}Pb$		15·5171	15·5166		15·5214		
$^{208}Pb/^{204}Pb$		38·149	38·145		38·179		
$^{176}Hf/^{177}Hf$		0·283230	0·283226		0·283227		

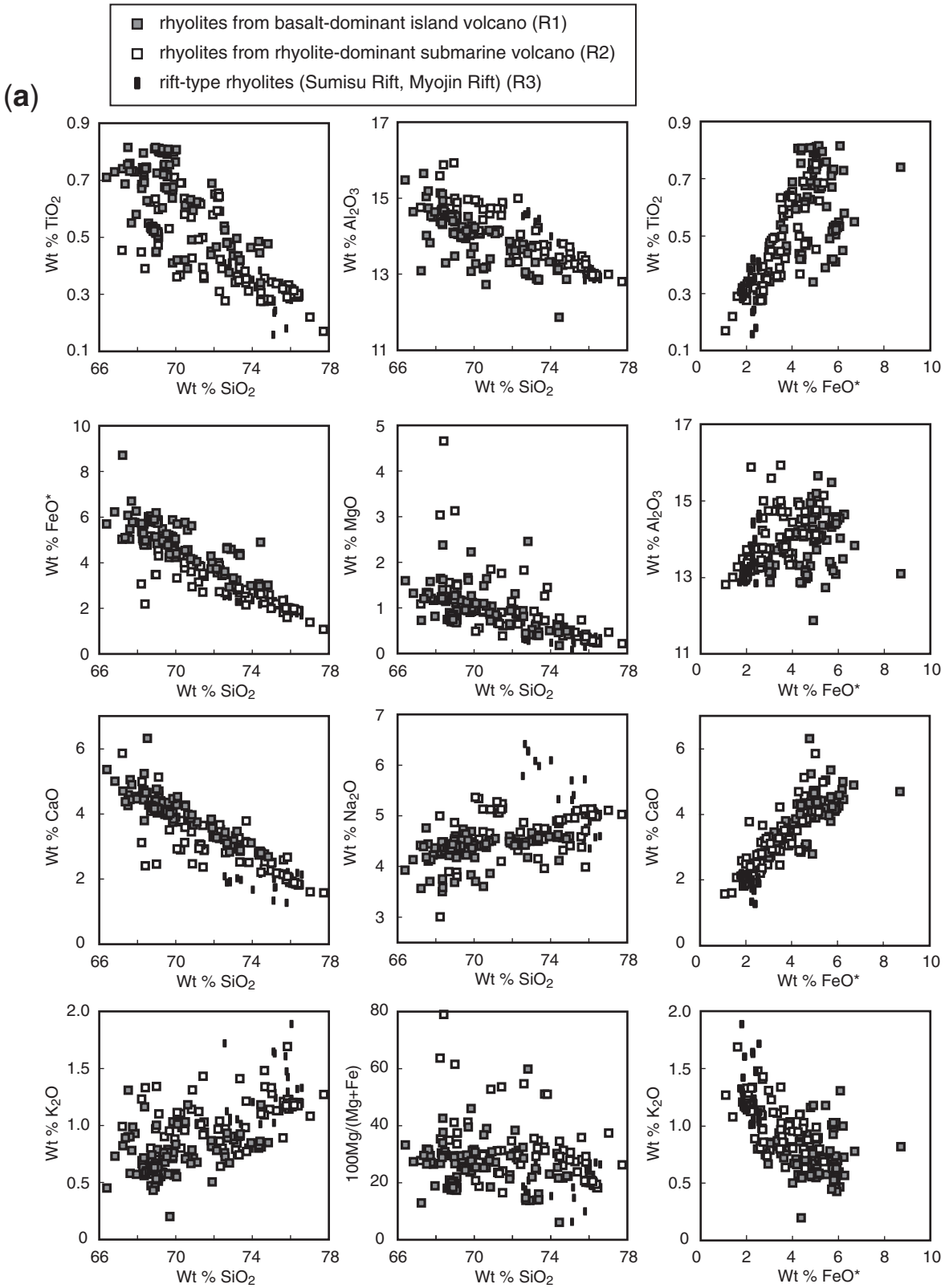

Fig. 4. Variation diagrams of rhyolites from basalt-dominant island volcanoes (R1), rhyolites from rhyolite-dominant submarine volcanoes (R2) and rift-type rhyolites (R3). The locations of R1 and R2, which alternate along the Izu–Bonin volcanic front, are shown in Figs 2 and 3. (a) Variation diagrams of wt % SiO_2 vs major element oxides (wt %) and Mg-number values [100Mg/(Mg + ∑Fe)] and those of wt % FeO* vs selected oxides (wt %). (b) Variation diagrams of wt % SiO_2 vs selected trace elements (ppm). (c) CaO/Al_2O_3 vs Mg-number of rhyolites from basalt-dominant volcanoes, those from rhyolite volcanoes, rift-type rhyolites and averages of Quaternary andesites and Oligocene andesites (see Fig. 17). (d) Wt % SiO_2 vs selected trace element ratios. Lines for arc-front basalts (AFB) show the averages of Quaternary arc-front basalts from Miyake-(jima) (Yokoyama *et al.*, 2003), Hachijo-(jima) (Ishizuka *et al.*, 2008), Sumisu (Tamura *et al.*, 2005) and Torishima (Tamura *et al.*, 2007). Oligocene mafic turbidites (OMT) and rift basalts (RB) show the averages from Gill *et al.* (1994) and Hochstaedter *et al.* (2001) and this study, respectively. Horizontal lines in plots of Zr/Sm, Hf/Sm, and Dy/Yb show the Cl-chondrite ratios, which are 25, 0·695 and 1·54, respectively (Palme & Jones, 2004).

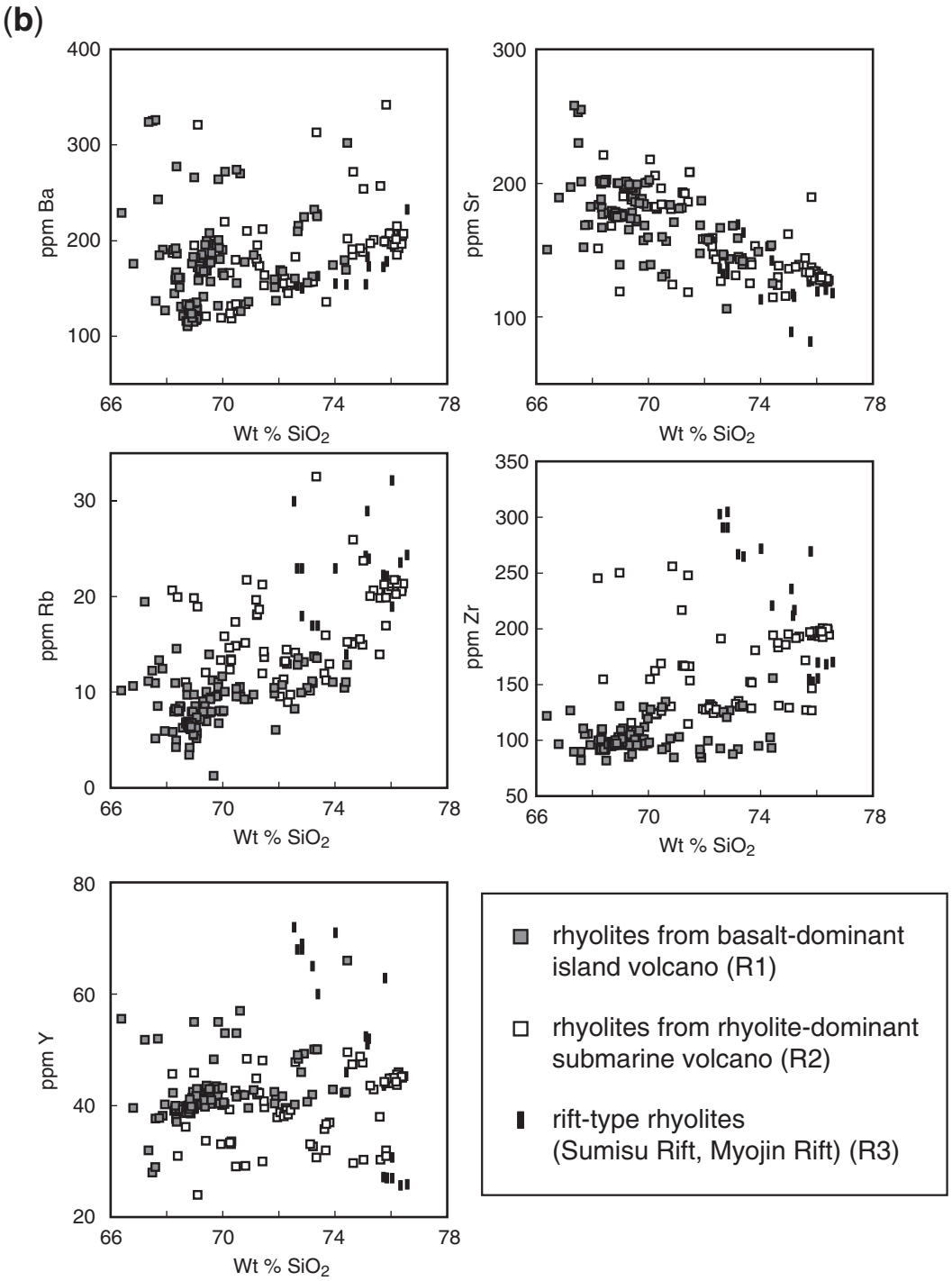

Fig. 4. Continued.

Rb and Zr contents but higher or similar Y. Consequently, CaO/Al_2O_3 and Zr/Y ratios roughly and clearly separate R1 from the other types. R2 and R3 are similar in major elements, except Na_2O, which may reflect a lower degree of partial melting for R3. The negative correlations between SiO_2 and Zr and Y in R3 reflect the variation between different rifts, not within them.

Figure 4c shows the variation of CaO/Al_2O_3 with Mg-number of rhyolites, which we relate to the anorthite (An) content [100Ca/(Ca + Na)] of their plagioclase.

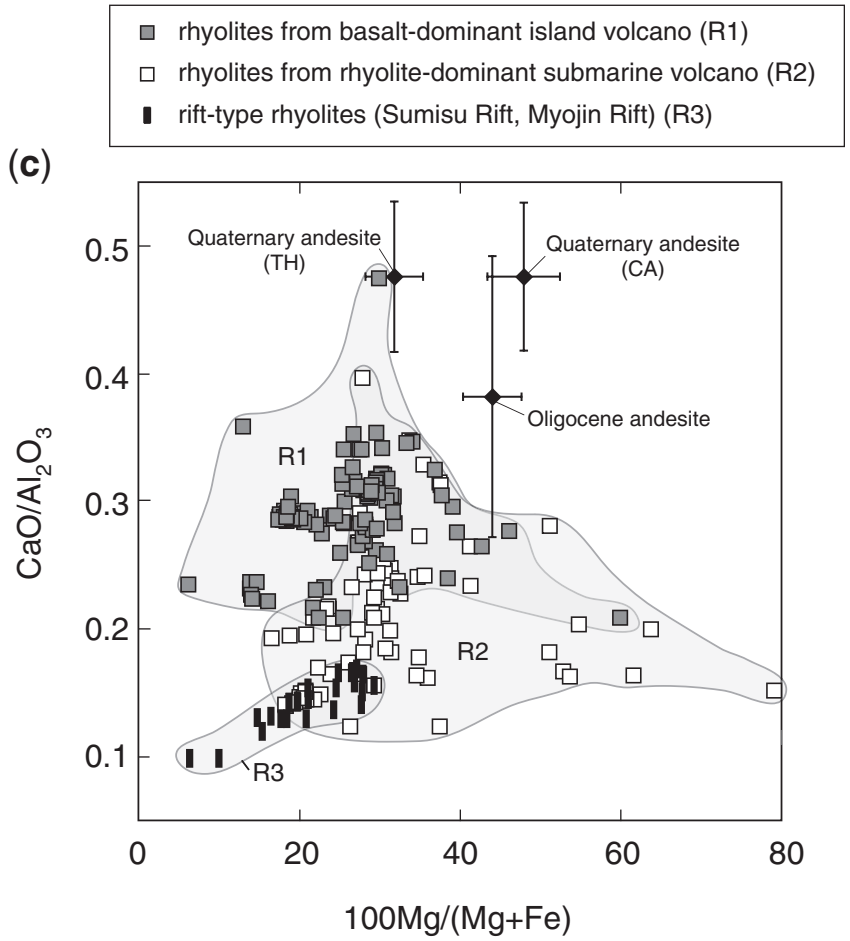

Fig. 4. Continued.

Rhyolites from basalt-dominant volcanoes have higher CaO/Al_2O_3 than those from rhyolite-dominant volcanoes, whereas R3 have the lowest ratios. R2 rhyolites also have higher Zr and lower Y contents than R1 rhyolites and they are clearly different in Zr/Y values (Fig. 4d), which is also illustrated by the Torishima–SW Torishima and Sumisu–South Sumisu pairs that we discuss below. We attribute the small number of rhyolites with Mg-numbers above 50 to mixing with a mafic component, something that seems most common in R2.

Figure 4d shows the variation of selected trace element ratios with SiO_2 content. Lines show the averages of the three possible mafic sources of rhyolites, which are Quaternary arc front basalts (AFB), Oligocene mafic turbidites (OMT) and Quaternary rift basalts (RB). AFB data are from Miyake (Yokoyama *et al.*, 2003), Hachijo (Ishizuka *et al.*, 2008), Sumisu (Tamura *et al.*, 2005) and Torishima (Tamura *et al.*, 2007). OMT values are from Gill *et al.* (1994). RB data are from Hochstaedter *et al.* (2001) and this study. The differences and relative orders between R1, R2 and R3 in Ba/La, Zr/Y and La/Yb are similar to differences between Quaternary arc front basalts, Oligocene mafic turbidites and Quaternary rift basalts and, therefore, possible rhyolite sources. In contrast, the difference in Zr/Sm and Hf/Sm may reflect differences in the processes of magma genesis.

Figure 5 shows the contrasting REE patterns between the different rhyolite types. R1 rhyolites have light REE (LREE)-depleted patterns (Fig. 5a), R2 rhyolites have LREE-enriched patterns (Fig. 5b) and R3 rhyolites have similar patterns to R2 rhyolites, but extend to higher concentrations (Fig. 5c). Figure 5d shows all three rhyolite types and their contrasting REE patterns. Figure 5e shows REE patterns of Quaternary Izu AFB from Hachijo, Miyake, Sumisu and Torishima volcanoes (Yokoyama *et al.*, 2003; Tamura *et al.*, 2005, 2007; Ishizuka *et al.*, 2008) and Fig. 5f shows both R1 rhyolites and AFB. Importantly, LREE-depleted patterns in R1 rhyolites (Fig. 5a) are sub-parallel to those of Quaternary arc front basalts and andesites from the Izu volcanic front

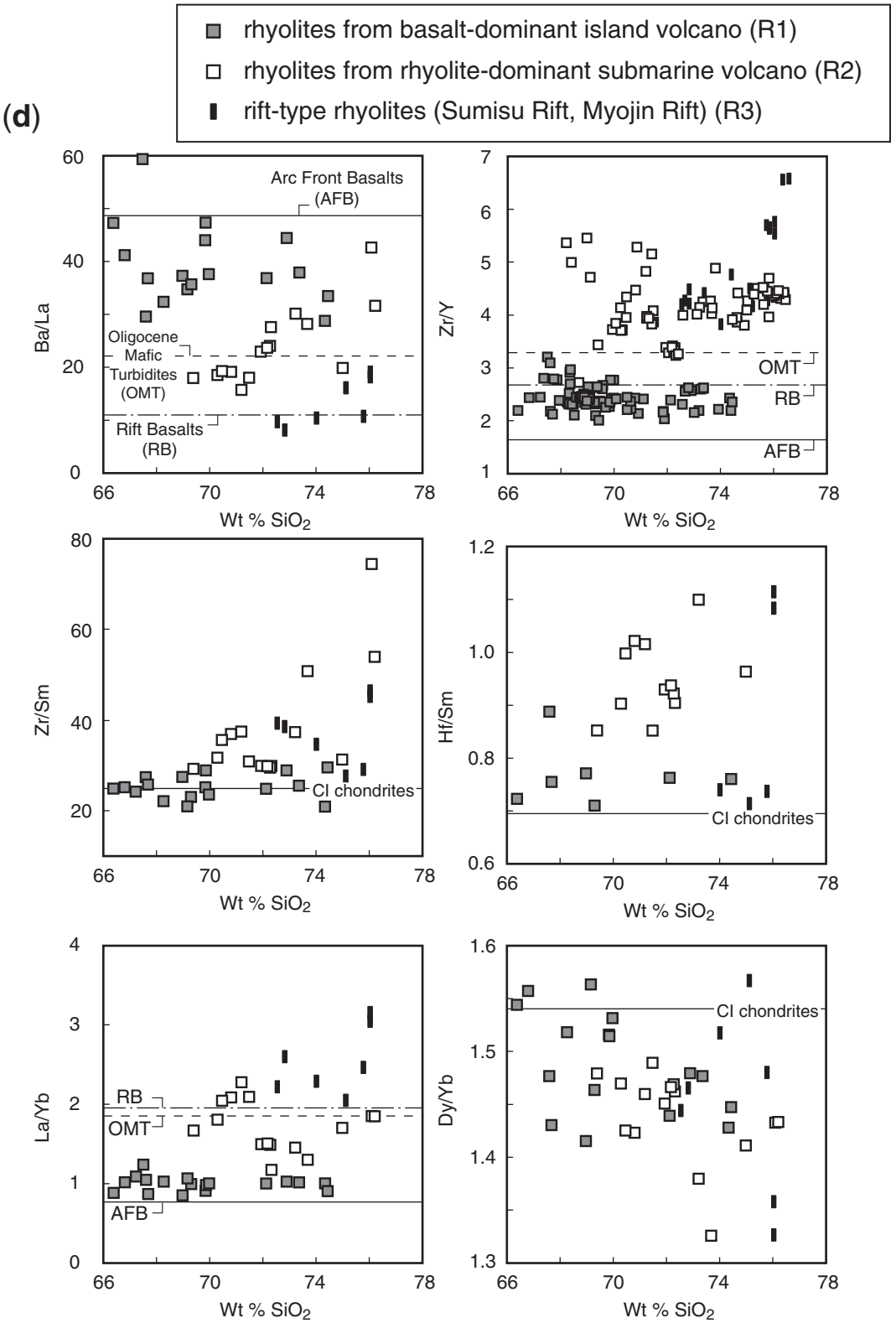

Fig. 4. Continued.

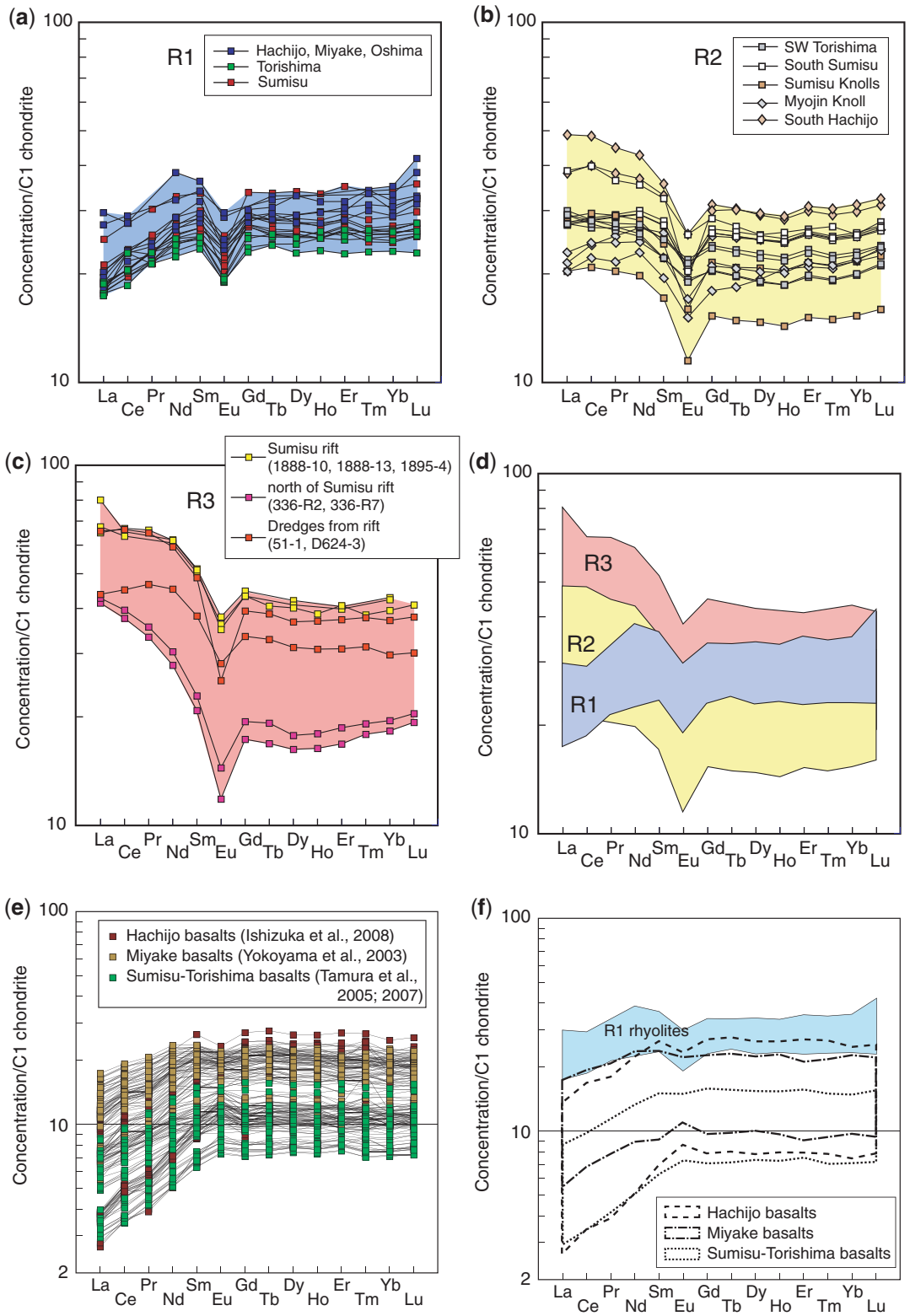

Fig. 5. REE patterns of (a) rhyolites from basalt-dominant volcanoes (R1), (b) rhyolites from rhyolite-dominant volcanoes (R2) and (c) rift-type rhyolites (R3). (d) Different REE patterns between R1 (blue field), R2 (yellow field) and R3 (red field). (e) REE patterns of Quaternary arc front basalts (AFB) from Miyake, Hachijo, Sumisu and Torishima. (f) REE patterns of R1 rhyolites and AFB, showing similar patterns depleted in LREE compared with middle REE and heavy REE. (g) La/Sm vs Dy/Yb of Quaternary arc front basalts (AFB), Quaternary rift basalts (RB) and Oligocene mafic turbidites (OMT). (h) La/Sm vs Dy/Yb of three kinds of rhyolites (R1, R2 and R3) compared with fields of AFB, RB and OMT.

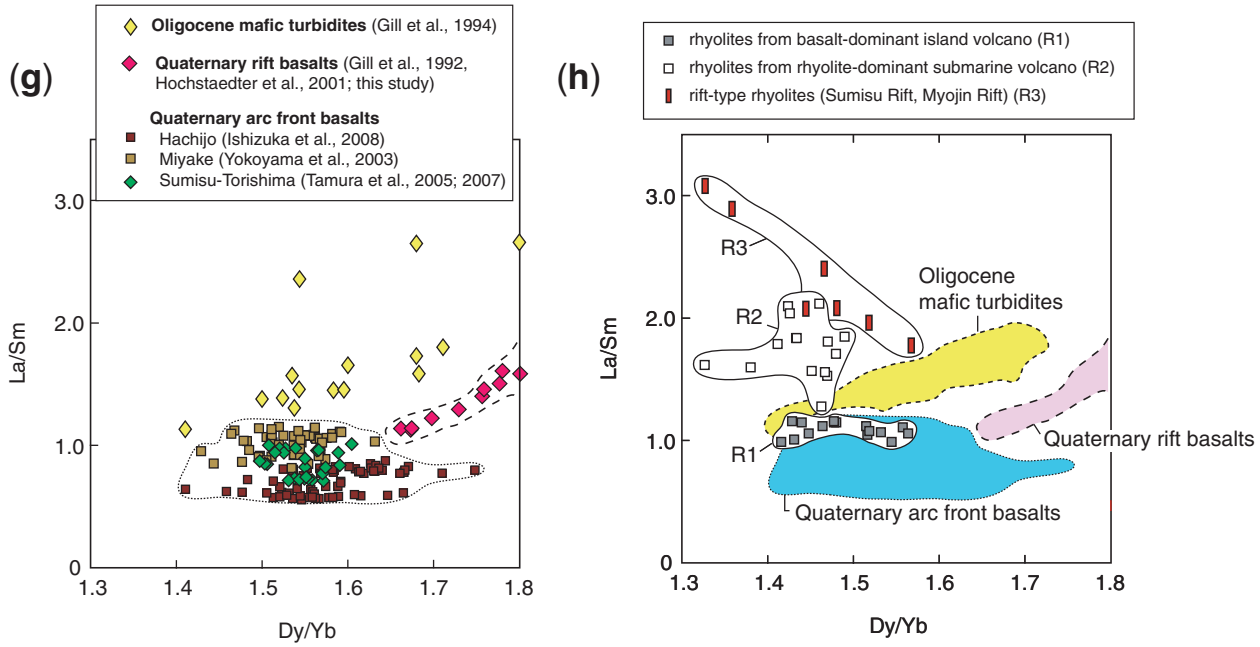

Fig. 5. Continued.

(e.g. Gill *et al.*, 1994; Shukuno *et al.*, 2006). The LREE-enriched patterns of the R2 rhyolites (Fig. 5b) differ from both those of R1 rhyolites and Quaternary frontal basalts. None have negative Ce anomalies and the average Eu anomaly of all three types is –20%. Figure 5g shows La/Sm vs Dy/Yb ratios of AFB, RB and OMT. Quaternary AFB have lower La/Sm compared with OMT and Izu rift basalts. Dy/Yb values have similar ranges within AFB and OMT, but RB have steeper REE patterns. La/Sm increases from R1 through R2 to R3 (Fig. 5h). The rhyolites overlap in Dy/Yb, but ratios in 50% of R1s are higher than in any of the R2s, whereas two of the R2s are lower than any of the R1s. R3s extend to the highest La/Sm and show a negative correlation between La/Sm and Dy/Yb that reflects the variation between rifts. All rhyolites have a restricted range of Dy/Yb at the low end of the range of their possible mafic sources. R1 overlaps more of the basalt field than R2, which may be consistent with more amphibole in the source of R2.

New Sr, Nd and Pb isotopic data for rhyolites from the Torishima Rift, SW Torishima, Torishima, South Sumisu, Sumisu, Myojin Rift, Myojin Knoll and South Hachijo are integrated with previously published data for Quaternary frontal volcanoes in the Izu–Bonin arc (Taylor & Nesbitt, 1988; Ishizuka *et al.*, 2003*a*, 2008; Yokoyama *et al.*, 2003; Tamura *et al.*, 2005) and the Sumisu Rift (Hochstaedter *et al.*, 1990*b*). Figure 6 shows along-arc Sr–Nd–Pb isotopic and Zr/Y ratios for lavas from frontal volcanoes, the Torishima–Sumisu–Myojin Rifts and the Oligocene arc. Results for basalts and rhyolites from basalt-dominant volcanoes and rifts overlap and are plotted together. Rhyolites from rhyolite-dominant volcanoes have lower $^{87}Sr/^{86}Sr$, $^{206}Pb/^{204}Pb$, $^{207}Pb/^{204}Pb$, $^{208}Pb/^{204}Pb$, and usually $^{143}Nd/^{144}Nd$ than lavas (basalt–rhyolite) from nearby basalt-dominant volcanoes (Fig. 6). Systematic along-arc variations in the isotopic composition of the mafic lavas of the Izu–Bonin arc, which have been reported by Taylor & Nesbitt (1998) and Ishizuka *et al.* (2003*a*), do not apply to the rhyolite volcanoes.

Lava, turbidite, and tephra samples from the Oligocene Izu arc all have lower Pb, Sr, and usually Nd isotope ratios than their Quaternary analogues (Gill *et al.*, 1994; Taylor & Nesbitt, 1998; Straub *et al.*, 2007). The difference may reflect a temporal change in the character of the recycled subducting sediment. Although the Oligocene dataset is small at present, it is consistent. The volcaniclastic materials may be derived from many different volcanoes. Even though the lower isotope ratios of the rhyolite volcanoes do not exactly overlap the existing data for Oligocene samples, their consistent offset from Quaternary values suggests derivation at least in part from Oligocene arc crust. It is possible, of course, that there are along-strike isotopic variations in the Oligocene arc too, such that the apparent similarity between the R2 rhyolites and Oligocene crust is fortuitous. However, additional data would be needed to test this hypothesis.

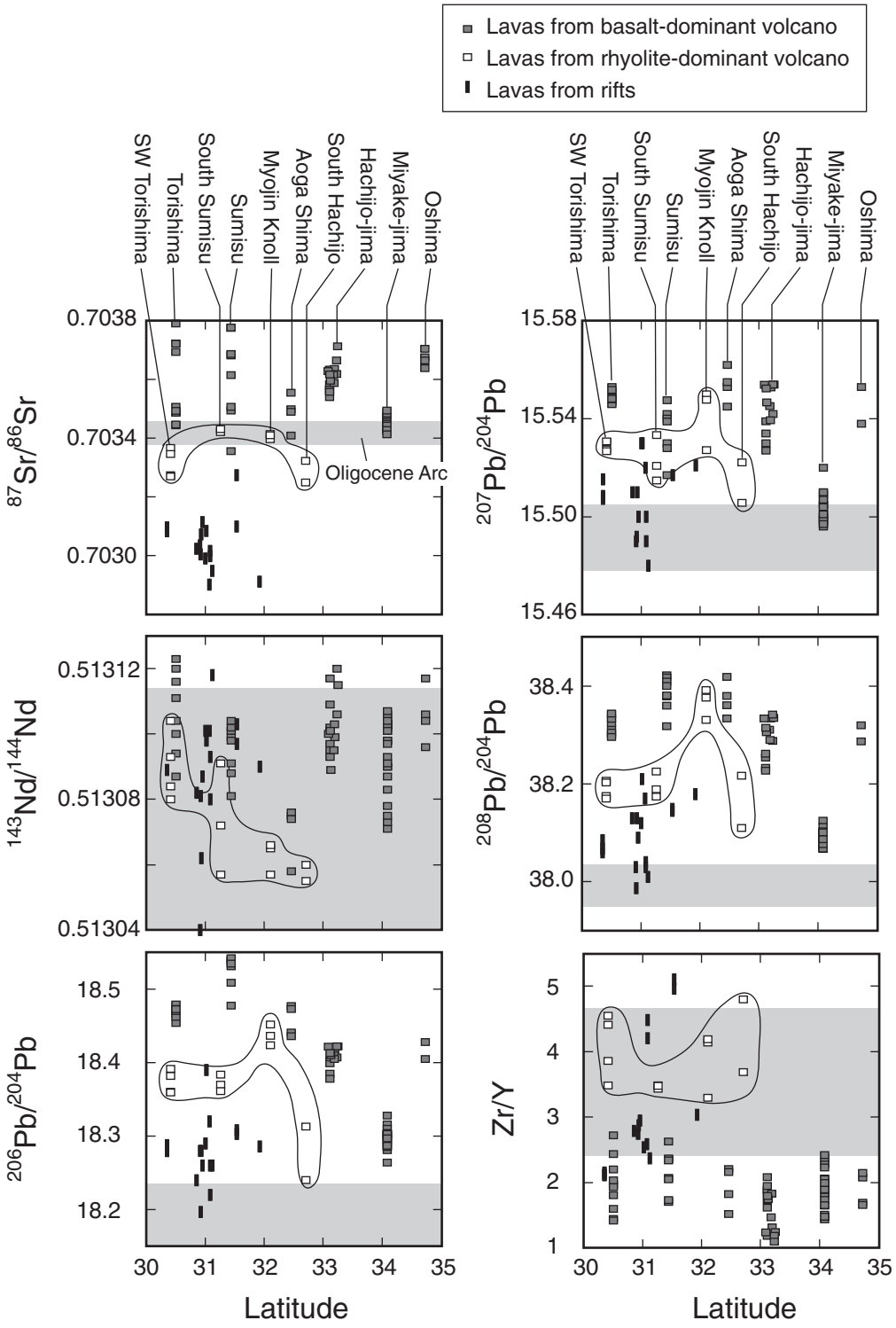

Fig. 6. Along-arc Sr–Nd–Pb isotopic and Zr/Y variations in lavas from frontal arc volcanoes and the Myojin–Sumisu–Torishima rifts, Izu–Bonin arc. Data from this study (SW Torishima, Torishima, South Sumisu, Myojin Knoll, South Hachijo, Torishima Rift, Sumisu Rift and Myojin Rift), Taylor & Nesbitt (1998), Ishizuka *et al.* (2003*a*) (Quaternary frontal volcanoes), Ishizuka *et al.* (2008) (Hachijo-jima submarine parts), Yokoyama *et al.* (2003) (Miyake-jima), and Hochstaedter *et al.* (1990b) (Sumisu Rift). The values for the Oligocene arc are from turbidites (Gill *et al.*, 1994), ODP Hole 792E (Taylor & Nesbitt, 1998) and tephras (Straub *et al.*, 2007).

The lower Sr and Pb isotope ratios of rhyolite volcanoes also are similar to those of the Plio-Pleistocene basalts from the backarc knolls (BAK) extensional zone behind the Izu volcanic front (Hochstaedter *et al.*, 2001; Ishizuka *et al.*, 2003*a*) (in this study, we make no distinction between backarc rift and backarc knoll basalts). Rhyolites and basalts from the Torishima–Sumisu and Myojin Rifts have the lowest Sr and Pb isotope ratios. Thus some rhyolites, especially R3 types, could be related genetically to Plio-Pleistocene basalts.

CASE STUDIES OF RHYOLITE FROM TWO RHYOLITE-DOMINATED VOLCANOES

To understand these differences better, we have studied two new examples of rhyolite-dominated volcanoes in detail (SW Torishima and South Sumisu). Figure 7 shows a bathymetric map of the frontal island volcanoes Myojinsho, Sumisu and Torishima, and the rifts just behind them. There is a dramatic decrease in middle crustal thickness along the 30 km distance from Sumisu to South Sumisu volcano (Fig. 3). Basalt–basaltic andesite (<55 wt % SiO_2) and dacite–rhyolite (66–74 wt % SiO_2) are the predominant eruptive products in the Sumisu caldera volcano (Tamura *et al.*, 2005; Shukuno *et al.*, 2006), whereas South Sumisu is dominated by rhyolites with ~75 wt % SiO_2. Torishima, at the other end of the spectrum, is a large volcano with a predominantly basaltic composition (Tamura *et al.*, 2007). There is a small knoll SW of Torishima, which is linked to the Torishima volcano by a linear topographic high (Fig. 7). Nishizawa *et al.* (2006) studied across-arc structural variations from Torishima toward the Shikoku basin to the west. Their profile shows that the middle crust is thick below Torishima volcano, and that it decreases in thickness westward toward the Torishima Rift near the SW Torishima Knoll. It thickens again toward Horeki seamount, a basaltic volcano located in the rear-arc.

Stratigraphic sections exposed on the rift wall of these two rhyolite-dominant submarine volcanoes (SW Torishima and South Sumisu) were surveyed and sampled using ROV *Hyper-Dolphin* aboard the R.V. *Natsushima* during JAMSTEC NT06-21 cruise in November 2006. Dive HD-616 studied SW Torishima from the bottom of the rift valley [2120 m below sea level (mbsl)] to 1132 mbsl (Fig. 8a). Dive HD-617 studied South Sumisu from the bottom of the rift valley (2110 mbsl) to 1386 mbsl (Fig. 8b). Figure 9 shows the lithologies exposed in SW Torishima and South Sumisu from the bottom to near the top of the sections, and Figure 10 shows schematic sections through these two rhyolite volcanoes interpreted based on the ROV observations and chemical analyses of the recovered rocks. Figure 11 compares stratigraphic chemical profiles of the submarine rocks with those of lavas from the Torishima and Sumisu volcanoes.

SW Torishima (Dive HD-616)

We collected rocks ranging from basaltic pillow lavas at the base (Fig. 9a) to rhyolite lava breccia near the top (Fig. 9f). Figure 9c shows that the lowest rhyolite breccia is overlain by a basalt flow, which changes upward into pillow lavas (Fig. 9d). Rhyolite pumice tuff, volcaniclastic rocks and breccia predominate from 1830 m to 1130 m (Fig. 9e and f). Figures 10 and 11 show that the rocks are bimodal in terms of SiO_2 content consisting of basalts (~50 wt % SiO_2) and rhyolites (~70 wt % SiO_2). Basaltic pillow lava at the base (~2100 m) and brecciated lavas at a depth of ~1800 m are differentiated (Mg-number = 40–50), and are similar to Torishima high-Zr basalts in terms of their Sr, Nd, and Pb isotope and Zr/Y ratios (Tamura *et al.*, 2007). On the other hand, primitive pillow lavas, which have Mg-number of 66–67, at a depth of ~1900–2000 m are similar to the Sumisu rift basalts (Hochstaedter *et al.*, 1990*a*, 1990*b*). Interestingly, although the rift basalts cover part of the surface of the SW Torishima rhyolites (Fig. 9c), they might not be related to the magmatism of SW Torishima (Fig. 10a). The rift wall of the South Basin of the Sumisu Rift was investigated by *ALVIN* Dive 1889 located between our two dives. It recovered 1·0–1·4 Ma rift basalts (Hochstaedter *et al.*, 1990*a*). However, ODP Site 788, just 5 km east of this rift wall, recovered only Pliocene rhyolite pumice and no basalt. It seems that the rift walls are locally covered by basalts that erupted in the rift but did not extend into the volcanic front.

South Sumisu (Dive HD-617)

Dive HD-617 (Fig. 8b) began on the Sumisu Rift floor, and documented lithologies on one of the steepest cliffs from the rift floor up to a point just west of the South Sumisu caldera. The bottom of the rift is thickly covered by fine, light-colored sediment, perhaps volcanic ash. No pillow lavas (as seen in Dive HD-616) were observed on the floor of the rift valley. The Sumisu Rift wall seems to expose the lower west flank of South Sumisu volcano, which consists mostly of massive rhyolite dikes that display beautiful columnar joints (Fig. 9g and h), and are chemically similar to the rhyolite from SW Torishima (Fig. 11b). The observed layering of fine tuff and coarser volcaniclastic rocks in parts of the section (Fig. 10b) is similar to that of the Mio-Pliocene Shirahama Group, Izu Peninsula (Cashman & Fiske, 1991; Tamura *et al.*, 1991). These rocks were possibly the basement of the South Sumisu volcano and were subsequently intruded by rhyolite dikes. Alternatively, given that the layered section seems to overlie the rhyolitic unit, it is possible that these stratified

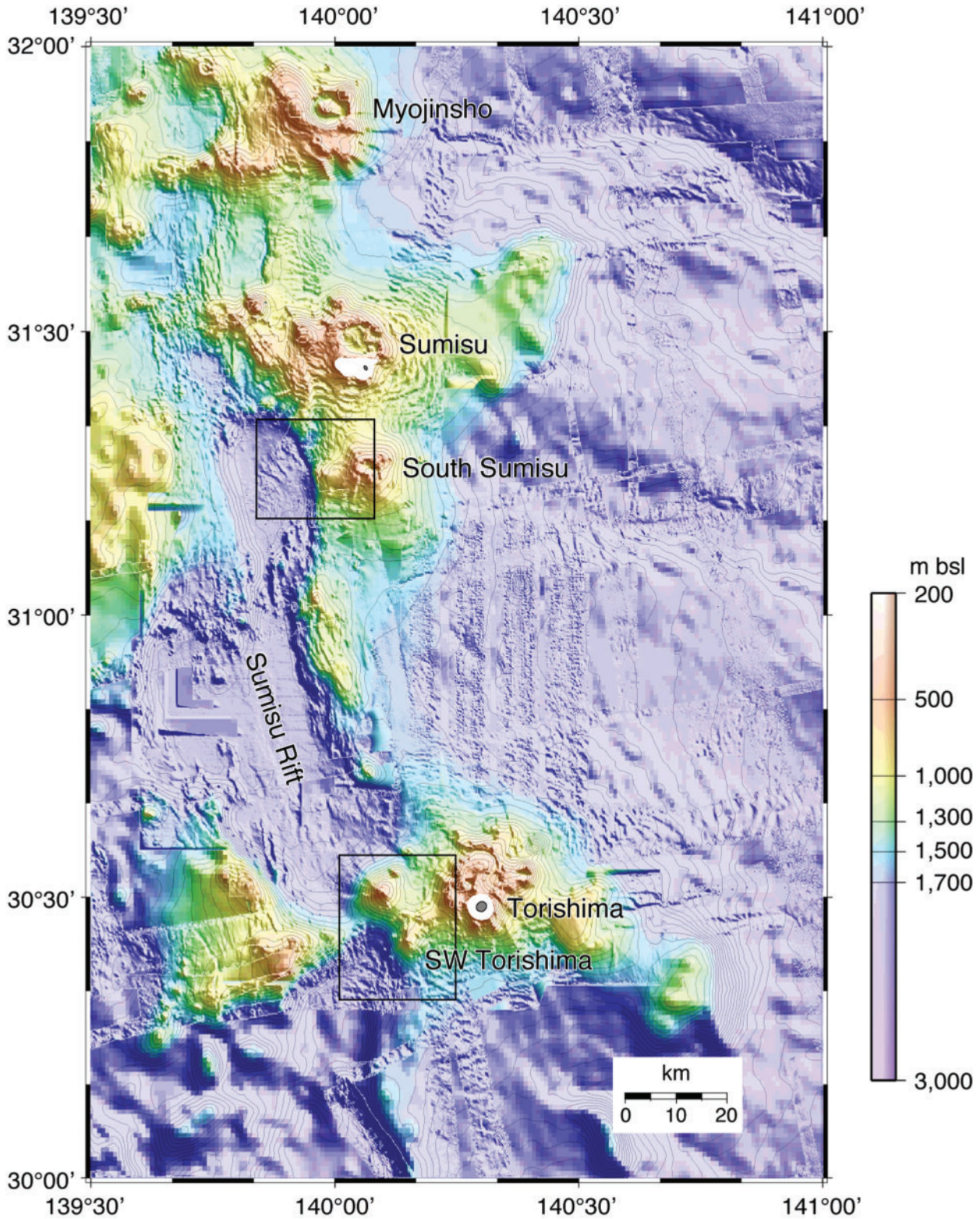

Fig. 7. Bathymetric map of the Myojinsho, Sumisu and Torishima area; contour interval 100 m. Data source: SeaBeam2100 and 2112 series, SeaBat and HS10 multi-narrow beam bathymetry by JAMSTEC research vessels obtained so far. JTOPO30 bathymetric dataset was compiled by Japan Hydrographic Department, Maritime Safety Agency, and consists of 30 min × 30 min gridded data. These datasets were smoothly merged using weighted means and simple averages using Generic Mapping Tools (GMT) software (Wessel & Smith, 1995). Details within the two rectangles showing the tracks of ROV *Hyper-Dolphin* are presented in Fig. 8.

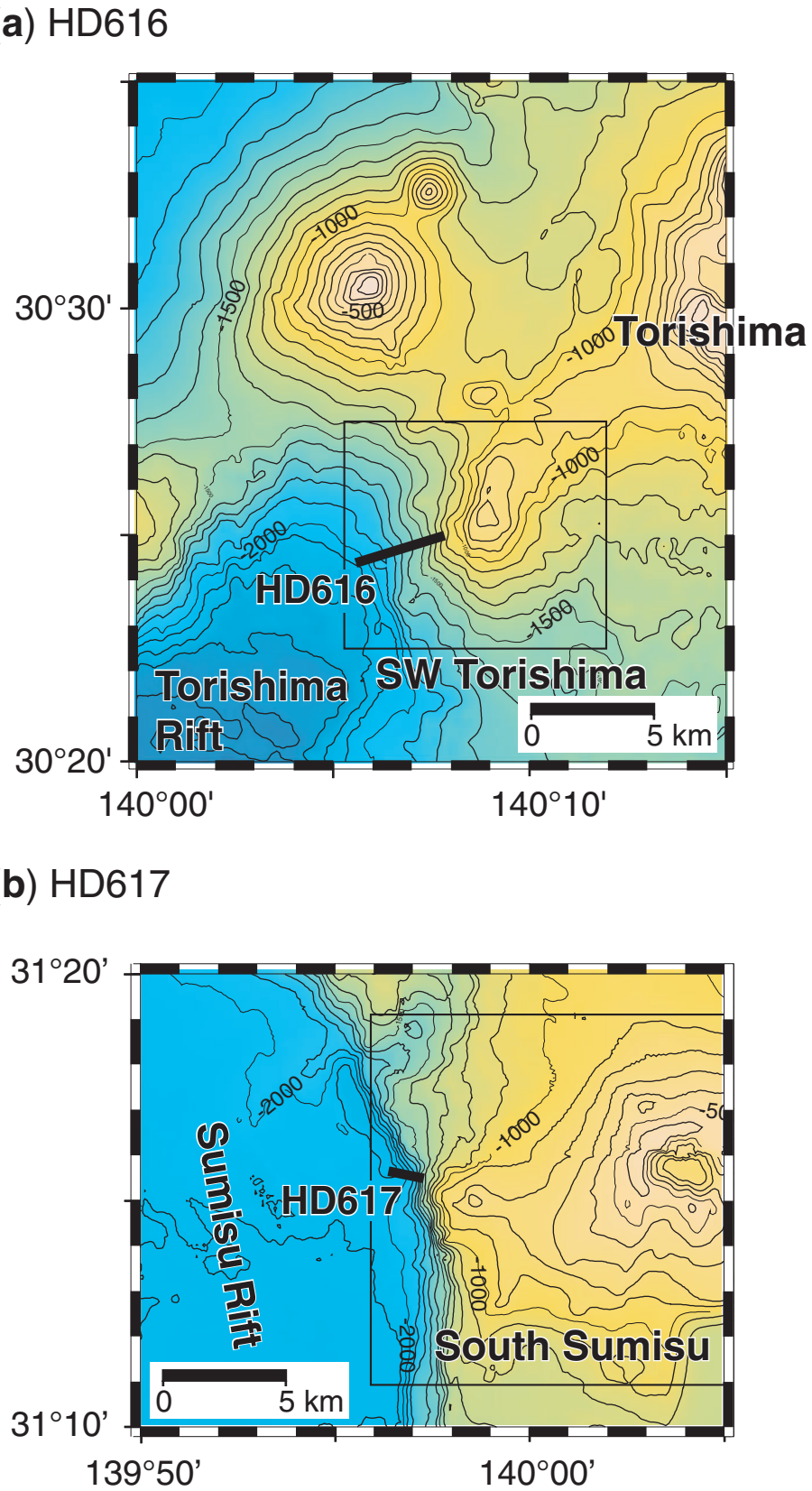

Fig. 8. The tracks of ROV *Hyper-Dolphin*. (a) HD-616 from 2130 to 1132 mbsl at the western wall of SW Torishima dissected by the Torishima Rift. (b) HD-617 from 2110 to 1386 mbsl at the western wall of South Sumisu dissected by the Sumisu Rift. Bathymetric contours are shown in meters below sea level.

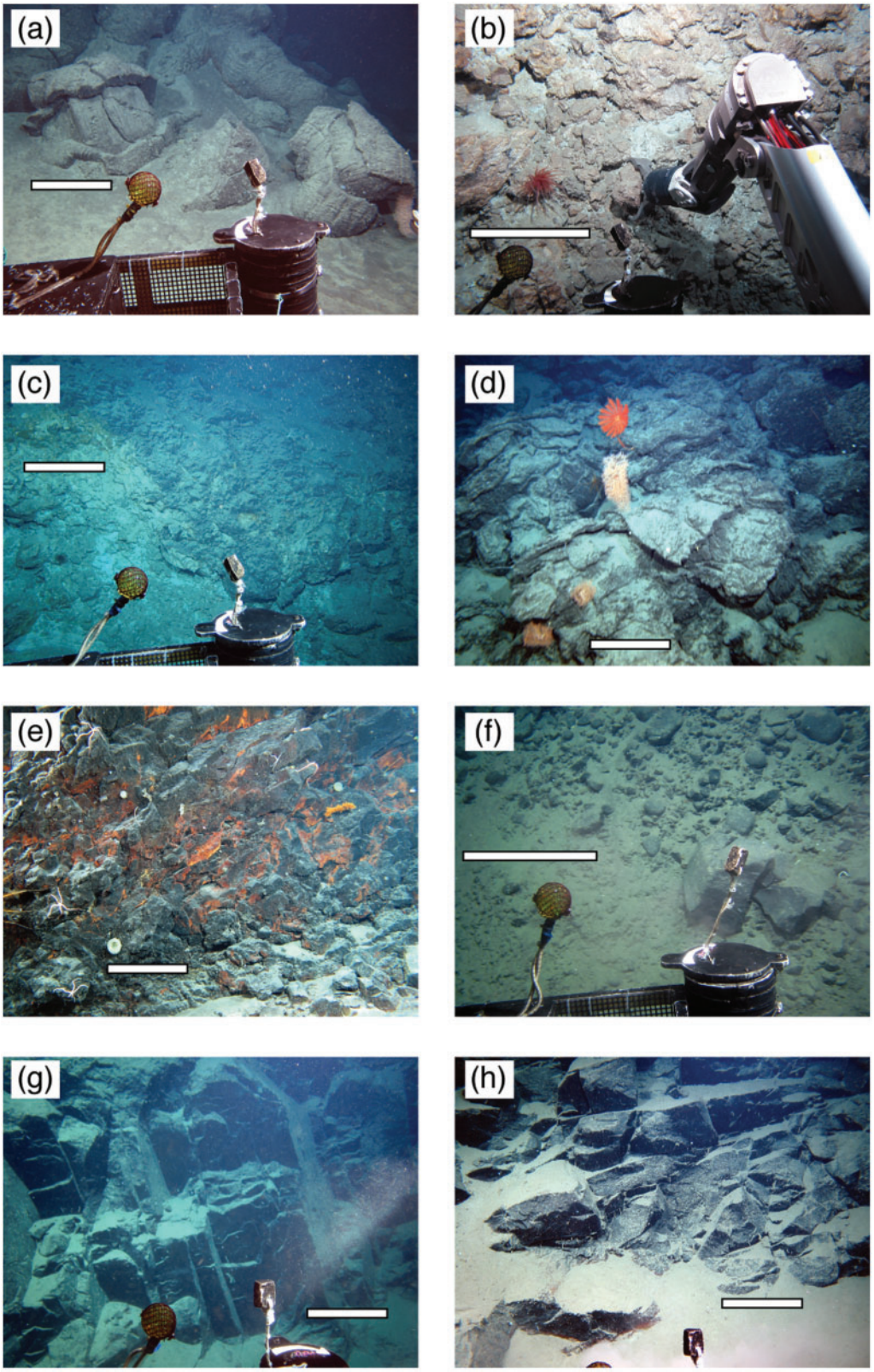

Fig. 9. Facies exposed in SW Torishima (HD-616) and South Sumisu (HD-617). Each scale bar represents ~50 cm. Collected sample numbers are shown in parentheses in captions. (a) HD-616, 2124 mbsl. Pillow lava at the bottom of the rift wall, which is chemically identical to the Torishima high-Zr basalt (HD-616-R01). (b) HD-616, 2057 mbsl. Rhyolite breccia (HD-616-R04). (c) HD-616, 2050 mbsl. Rift basalt lava flow (right) covers rhyolite breccia (left). (d) HD-616, 1957mbsl. Pillow lavas having affinity to rift-basalt (HD-616-R07). (e) HD-616, 1831 mbsl. Massive basalt dike? Similar to Torishima high-Zr basalt (HD-616-R09). (f) HD-616, 1381 mbsl. Rhyolite monomictic lava breccia (HD-616-R15). (g) HD-617, 1806 mbsl. Massive rhyolitic coherent unit with well-developed columnar joints (HD-617-R06). (h) HD-617, 1743 mbsl. Massive rhyolitic coherent unit (HD-617-R08).

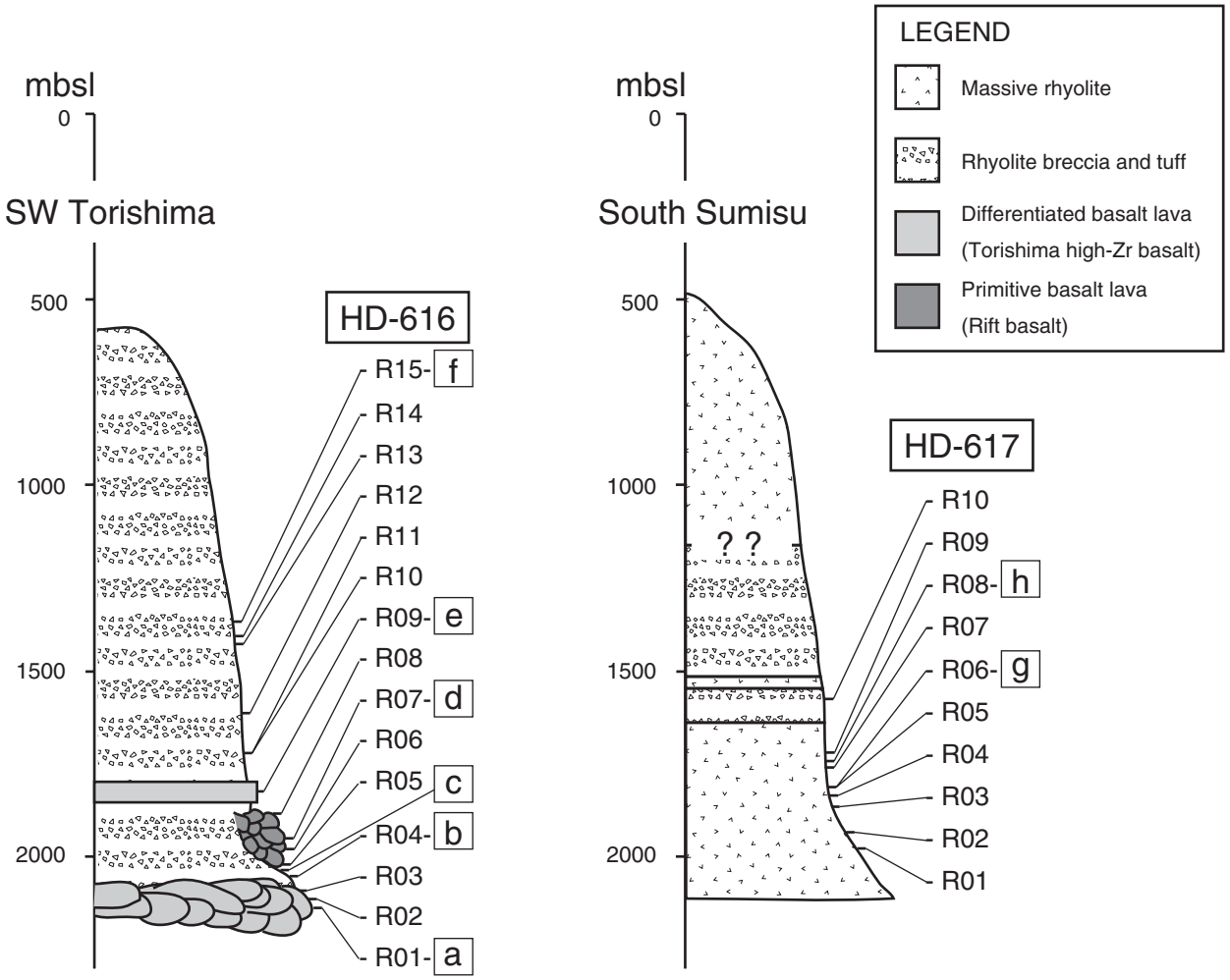

Fig. 10. Schematic observations and interpretation of cross-sections of SW Torishima and South Sumisu. Samples recovered from each section are shown. Letters a–h correspond to facies in Fig. 9.

volcanic rocks are related to the eruption of the South Sumisu volcano after or during emplacement of the rhyolite dikes.

Bulk-rock and mineral chemistry

Rhyolites from SW Torishima (69·4–70·8 wt % SiO_2) are slightly lower in SiO_2 content than those from South Sumisu (71·9–72·3 wt % SiO_2, Fig. 11). Rhyolites from Torishima and Sumisu have wider ranges in SiO_2 content and Mg-number, and the same isotopic range as the basalts from these volcanoes; the two rock types are therefore plotted together. Torishima and Sumisu basalts and rhyolites are significantly different in their Sr, Nd and Pb isotope composition from rhyolites from SW Torishima and South Sumisu (Fig. 11). In all cases the isotope ratios are higher in lavas from Torishima and Sumisu volcanoes. Zr/Y values also are consistently higher in SW Torishima and South Sumisu rhyolites than in the Torishima and Sumisu lavas.

Rift basalts recovered in HD-616 from SW Torishima have Mg-number of ~70; these are much more primitive than the Torishima and Sumisu basalts (Mg-number 40–60), and have significantly lower $^{87}Sr/^{86}Sr$, $^{206}Pb/^{204}Pb$, $^{207}Pb/^{204}Pb$ and $^{208}Pb/^{204}Pb$ ratios compared with the arc lavas of Torishima and Sumisu. These values are similar to those for Sumisu Rift basalts recovered several tens of kilometers to the north (Hochstaedter *et al.*, 1990*b*). Rhyolites from SW Torishima and South Sumisu are between the rift basalts and Torishima and Sumisu lavas in terms of their Sr and Pb isotope compositions (Fig. 11). Rift basalts have similar Zr/Y to Torishima and Sumisu lavas and much lower values than in rhyolites from SW Torishima and South Sumisu. These differences between the SW Torishima–South Sumisu rhyolites and the

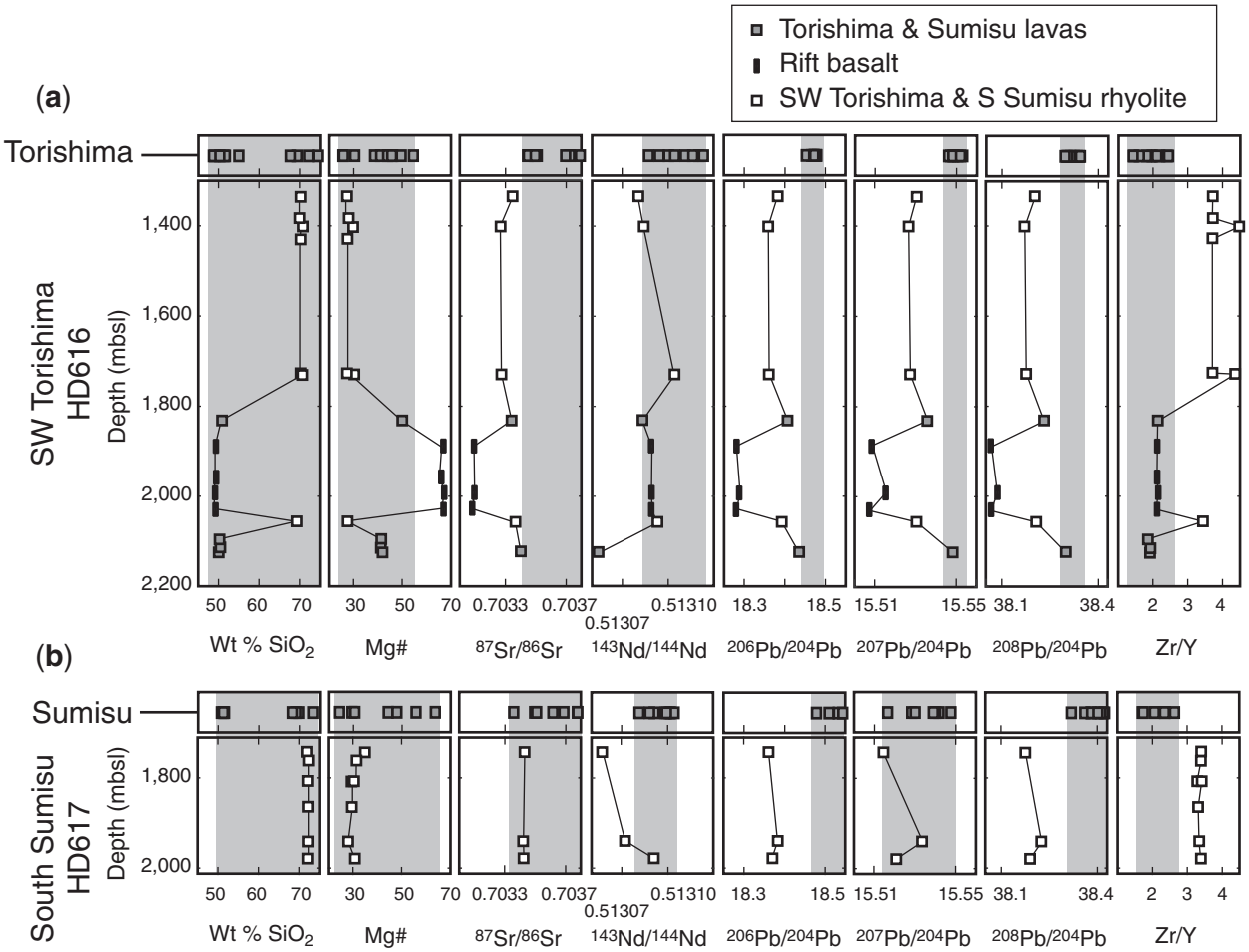

Fig. 11. Water depth vs silica content, Mg-number, isotope ratios ($^{87}Sr/^{86}Sr$, $^{143}Nd/^{144}Nd$, $^{206}Pb/^{204}Pb$, $^{207}Pb/^{204}Pb$, and $^{208}Pb/^{204}Pb$), and Zr/Yof rocks collected from (a) Dive HD-616 at SW Torishima and (b) Dive HD-617 at South Sumisu. Torishima and Sumisu are large basalt-dominant volcanoes and representative samples from them are shown at the top of each diagram. Isotope and Zr/Y ratios are the same for their basalts and rhyolites. The ranges of Torishima and Sumisu rhyolites are shown by the grey bands. HD-616 recovered three rock types: rift basalts, Torishima high-Zr basalts, and SW Torishima rhyolites. HD-617 recovered only South Sumisu rhyolites. Rhyolites from SW Torishima and South Sumisu have similar Sr, Nd and Pb isotope compositions and Zr/Y, but they are different from the rhyolites of Sumisu and Torishima. In most cases the isotope ratios are higher and Zr/Y values are lower in rhyolites from Torishima and Sumisu volcanoes.

Torishima–Sumisu rhyolites are generally seen between rhyolite-dominant volcanoes and basalt-dominant volcanoes as shown in Fig. 6.

All South Sumisu and SW Torishima rhyolites have the same phenocryst assemblage, consisting of a few volume per cent of euhedral to subhedral plagioclase, orthopyroxene, clinopyroxene and opaque minerals. This phenocryst assemblage is the same as that of the Sumisu dacites and rhyolites (Shukuno *et al.*, 2006). Figure 12 shows histograms of clinopyroxene, orthopyroxene and plagioclase composition for (a) Sumisu dacites based on the data of Shukuno *et al.* (2006), (b) SW Torishima rhyolites, and (c) South Sumisu rhyolites. The rhyolites from SW Torishima and South Sumisu have a limited and similar range in mineral compositions. These compositions are plotted together and compared with the dacites of Sumisu in Fig. 13. The relationship in Mg-number between augite and orthopyroxene is similar in all three cases (Fig. 13a), although Sumisu has a wider range. On the other hand, the relationship between the An content [100Ca/(Ca + Na)] of plagioclase and the Mg-number of orthopyroxene (and augite) is different between basalt-dominant Sumisu and rhyolite-dominant South Sumisu and SW Torishima (Fig. 13b). At a similar An content ($An_{\sim 50}$), lavas from the latter two have more magnesian orthopyroxene. We attribute the difference to the bulk composition of the melt because the plagioclase An content correlates positively with the CaO/Al_2O_3 of the bulk-rocks; the CaO/Al_2O_3 values of the South Sumisu and SW Torishima lavas are lower than those of the Sumisu rhyolites (Fig. 13d). Generally, rhyolites

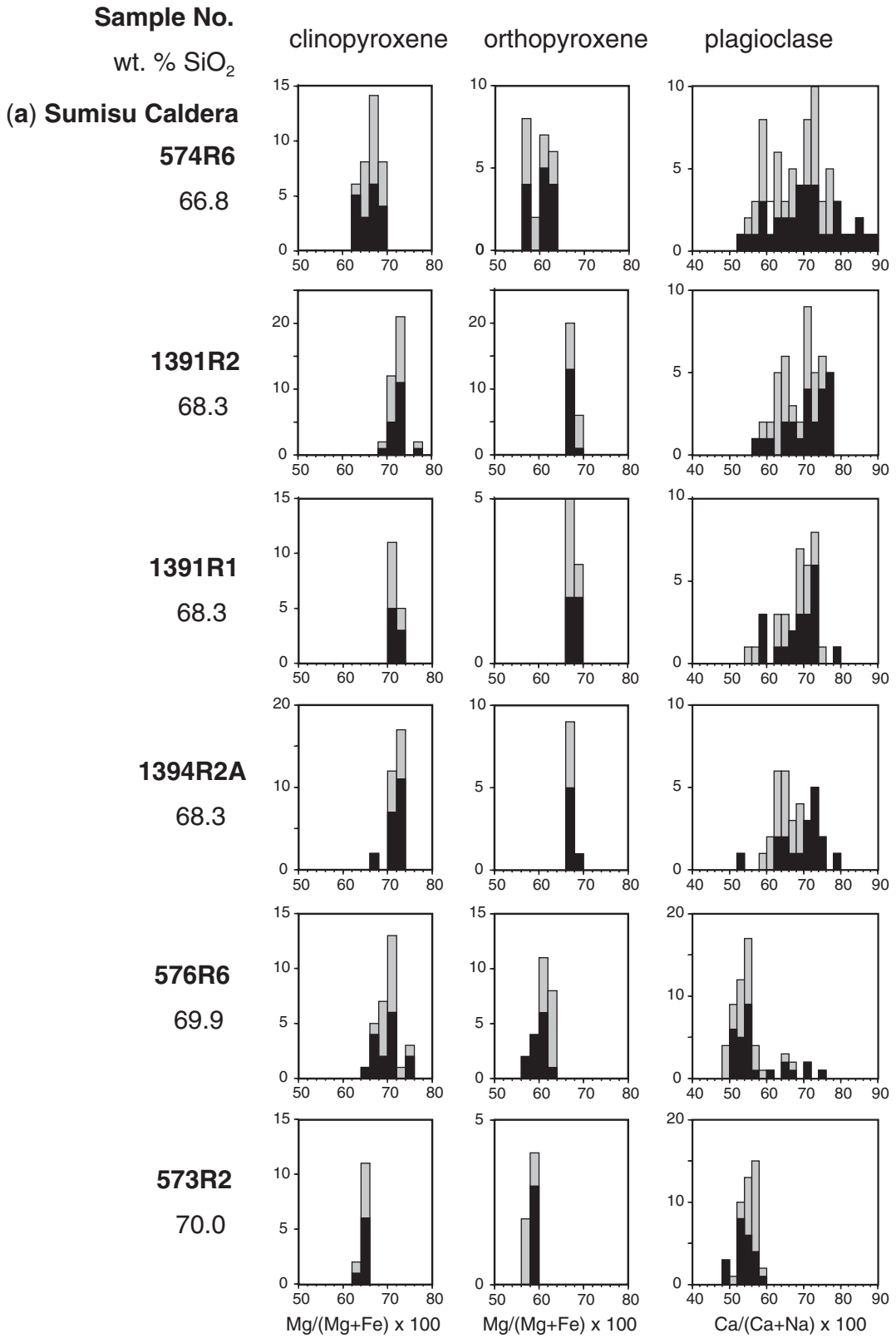

Fig. 12. Frequency distribution diagrams for core (black) and rim (grey) compositions of clinopyroxene, orthopyroxene and plagioclase phenocrysts in lavas from (a) the Sumisu caldera, (b) SW Torishima and (c) South Sumisu.

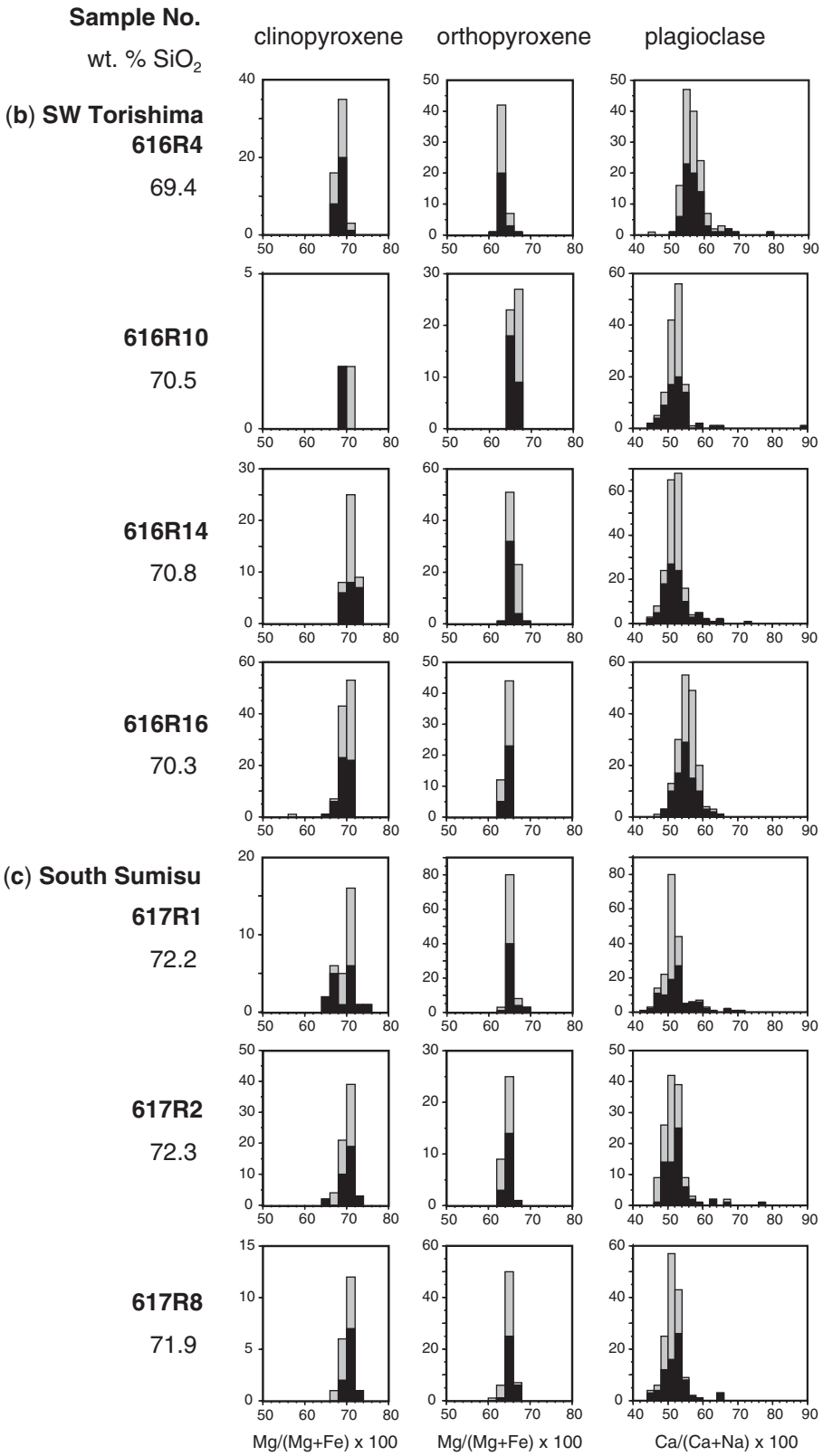

Fig. 12. Continued.

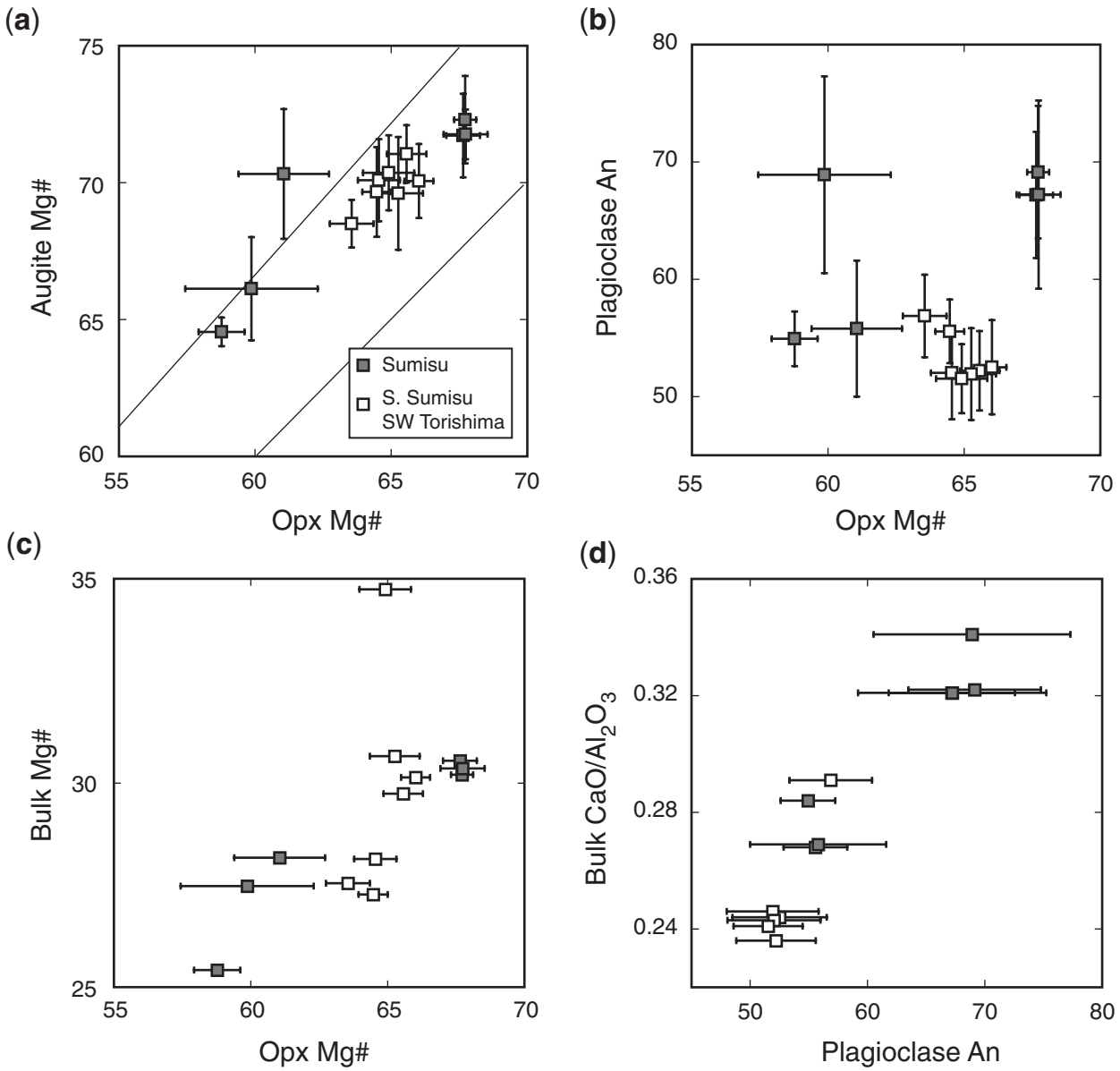

Fig. 13. Relationships among phenocryst and bulk-rock compositions in Sumisu rhyolites and rhyolites from South Sumisu and SW Torishima. Phenocryst compositions represent averages ± 1 SD from respective rhyolite lavas shown in Fig. 12. (a) Mg-number of augite vs Mg-number of orthopyroxene. (b) An [100Ca/(Ca + Na)] of plagioclase vs Mg-number of orthopyroxene. (c) Mg-number of bulk-rock vs Mg-number of orthopyroxene. (d) CaO/Al_2O_3 of bulk-rock vs An content of plagioclase.

from rhyolite-dominant volcanoes are lower in CaO/Al_2O_3 than those from basalt-dominant volcanoes (Fig. 4c).

GENESIS OF IZU ARC RHYOLITES

Felsic magmas can originate from two end-member processes: by fractional crystallization of basaltic or andesitic parents; or by partial melting of basaltic, andesitic, or sedimentary sources. Apart from sediment melts, these options are notoriously difficult to distinguish between. Because the Izu rhyolites lack evidence of non-volcanic sedimentary sources yet are abundant and diverse, we explore the possibility that the differences between rhyolite types reflect differences in their igneous parents or sources.

Middle crust andesite sources for rhyolites

Basalts, andesites, dacites and R1 rhyolites from the basalt-dominated Sumisu caldera volcano all have similar REE patterns and Sr–Nd–Pb isotope ratios, indicating that they are genetically related and retain characteristics inherited from a parental basalt magma derived from the mantle in the Quaternary. Whether this relationship is via

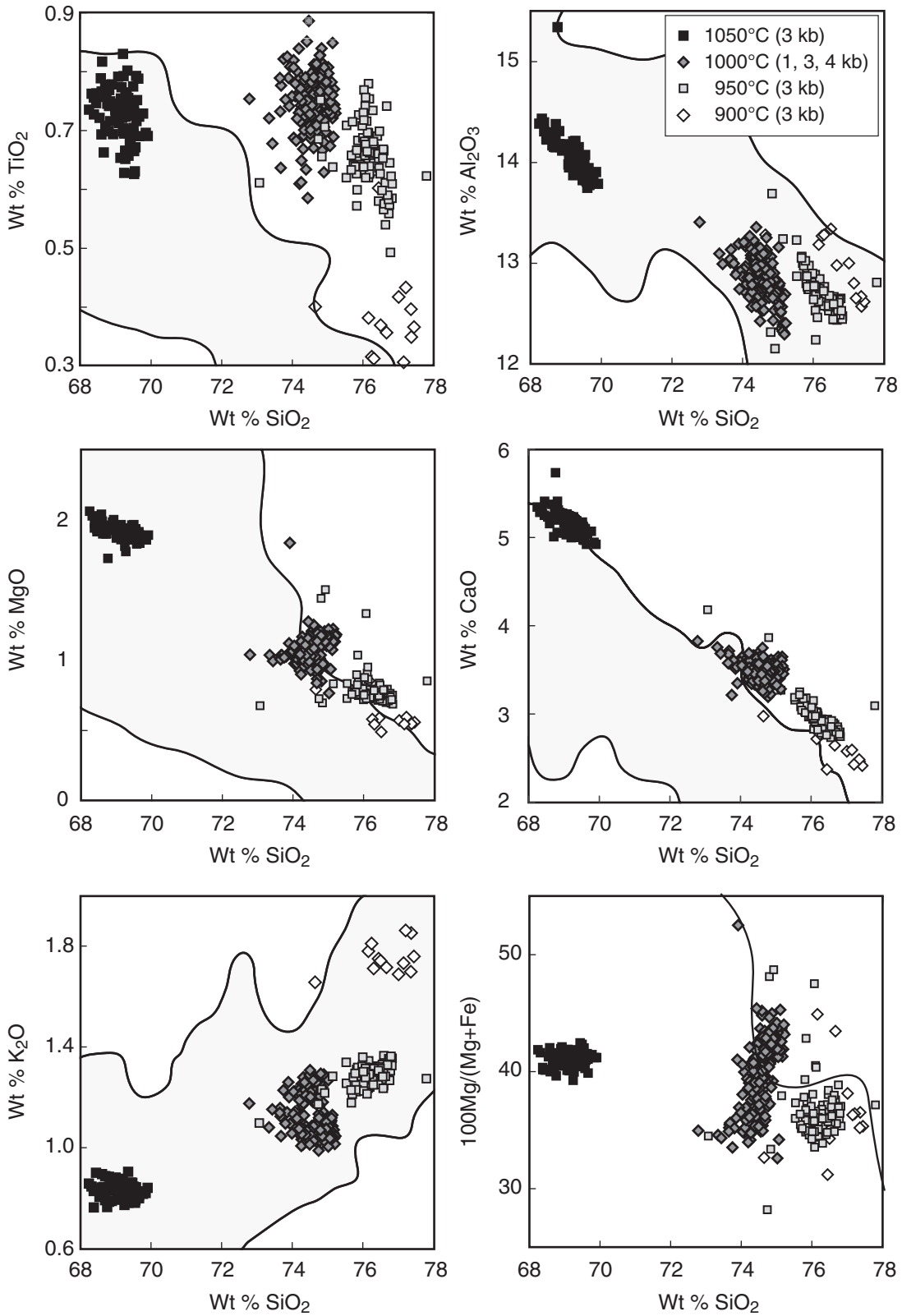

Fig. 14. Experimentally produced melts of Tanzawa tonalite (62 wt % SiO_2). Data from Shukuno *et al.* (2006) and T. Suzuki (Electronic Appendix Table 2). Shaded area in each panel represents data for Izu–Bonin rhyolites.

fractional crystallization or partial melting and melt segregation is uncertain, but several lines of evidence argue against fractional crystallization. Andesites are less abundant than dacites and rhyolites. Mass-balance calculations between basalt and andesite, in which phenocryst phases are subtracted from basalts to produce andesites, are unsuccessful (Shukuno *et al.*, 2006). Some andesites contain Fo-rich olivines, andesites and dacites contain sieve-textured plagioclase and reversely zoned orthopyroxenes, and there are temperature increases of ~200°C from core to rim in orthopyroxene phenocrysts based on two-pyroxene thermometry (Sumisu andesite ~900 to 1100°C and dacite ~800 to 1000°C) (Shukuno *et al.*, 2006). These observations suggest magma mixing in the andesites and are inconsistent with simple fractional crystallization from basalt through andesite to rhyolite. However, they are consistent with remobilization of an andesite mush as has been envisaged in the Adamello massif, Italy (Blundy & Sparks, 1992), the Lascar volcano, Chile (Matthews *et al.*, 1999), the Soufrière Hills volcano, Montserrat (Murphy *et al.*, 2000; Couch *et al.*, 2001; Harford & Sparks, 2001), the Daisen volcano (Tamura *et al.*, 2003) and the Oto-Zan lava flows on Shodo-Shima Island (Tatsumi *et al.*, 2006), SW Japan.

A second reason for believing that rhyolites are derived from andesitic sources is that the middle crust in the Izu arc has a V_p of 6·0–6·8 km/s at depths between 5 and 20 km (Kodaira *et al.*, 2007*a*, 2007*b*). Based on a comparison with the measured seismic velocities of samples of Tanzawa tonalite (Kitamura *et al.*, 2003), the upper part of the Izu middle crust ($V_p = 6{\cdot}0$–$6{\cdot}5$ km/s) seems to consist of rocks with high SiO_2 contents (>64 wt % SiO_2), and the lower part of the middle crust ($V_p = 6{\cdot}5$–$6{\cdot}8$ km/s) consists of rocks of intermediate composition (54–63 wt % SiO_2). The southern part of the Izu–Bonin arc has a thinner total crust than the northern part, but the ratio of middle crust to total crust in the south is similar to that below the basalt volcanoes in the north (Kodaira *et al.*, 2007*b*). In contrast, the crust below the rhyolite volcanoes in the north has relatively less middle crust (Kodaira *et al.*, 2007*a*, 2007*b*). We therefore infer that the middle crust below rhyolite volcanoes was originally thicker than at present. If so, then the observation that rhyolite-dominant volcanoes are underlain by thinner middle crust (Fig. 3) is consistent with partial melting of andesite because production of rhyolite from andesite would decrease the thickness of andesitic middle crust and increase the thickness of mafic restite in the lower crust.

Although we prefer andesitic sources for rhyolitic magma for the reasons given above, we cannot exclude the possibility that some rhyolites are derived from basalt, either directly via fractional crystallization or indirectly by partial melting. Our main observation is that the three rhyolite types cannot be derived from the same source, and we argue below that R1 rhyolites at island volcanoes are derived from Quaternary sources (basaltic or andesitic) whereas R2 and R3 rhyolites from submarine calderas and rifts are derived from Oligocene sources.

Dehydration melting of Izu–Bonin tonalite (SiO_2 ~ 60 wt %) at 3 kbar

The Tanzawa complex is a part of the Izu–Bonin arc crust that has been obducted onto Honshu, and is considered to be chemically similar to the middle to upper crust of the Izu–Bonin arc (Kawate & Arima, 1998). Kitamura *et al.* (2003) measured elastic wave velocities of tonalites collected from Tanzawa. Tonalites with >64 wt % SiO_2 and 54–63 wt % SiO_2 show seismic velocities consistent with the upper and lower part of the middle crust, respectively (Kodaira *et al.*, 2007*a*). Thus, the Tanzawa tonalite is consistent with the geophysical characteristics of the Izu–Bonin arc middle crust. Shukuno *et al.* (2006) showed that dehydration melting of Tanzawa tonalite (SiO_2 ~ 60 wt %) produces rhyolitic melts broadly similar to the rhyolites at Sumisu caldera; the experimental melt compositions are given in Electronic Appendix Table 2. Dehydration partial melting of this andesitic source can produce melts ranging from high-silica rhyolite (76–78 wt % SiO_2) at 900°C to dacite (68–70 wt % SiO_2) at 1050°C (Fig. 14), leaving a two-pyroxene gabbro residuum. Degrees of melting range from ~20% at 900°C to ~50% at 1050°C. The Mg-number values of the melts do not change very much, but SiO_2 and K_2O contents decrease and Al_2O_3, FeO, and CaO increase with increasing melting temperature (Fig. 14). Two-pyroxene thermometry data for the Sumisu dacites and rhyolites suggest temperatures of 850–1050°C; this result is consistent with the experimental melting temperatures if these magmas were produced by dehydration partial melting of tonalite (Shukuno *et al.*, 2006). The TiO_2, MgO and CaO contents of the experimental high-silica rhyolites (>73 wt % SiO_2) are higher than those of the actual rhyolites (R1, R2 and R3) (Fig. 14). Equilibration with amphibole during crystallization or melting seems to play a more important role in the petrogenesis of R2 than in R1 or the amphibole-free experiments (Shukuno *et al.*, 2006). Sm is more compatible than Zr and Hf in amphibole, and thus equilibration with amphibole would explain the higher (supra-chondritic) Zr/Sm and Hf/Sm ratios in R2, and the overall negative correlation between Dy/Yb and SiO_2 (Fig. 4d). The Dy/Yb systematics noted generally for arc magmas (Davidson *et al.*, 2007) are difficult to apply, but all the rhyolites have a restricted range of Dy/Yb values that lie at the low end of values for their potential mafic sources, and R1 overlaps more of the basalt field than R2 (Fig. 5h). This is consistent with more amphibole in the source of R2.

Figure 15 shows the relationship between experimental melting temperatures, CaO/Al_2O_3, Mg-number and melt fraction. At 3 kbar, Mg-number is constant at ~20–40% melting, but CaO/Al_2O_3 increases from about 0·2 to 0·3.

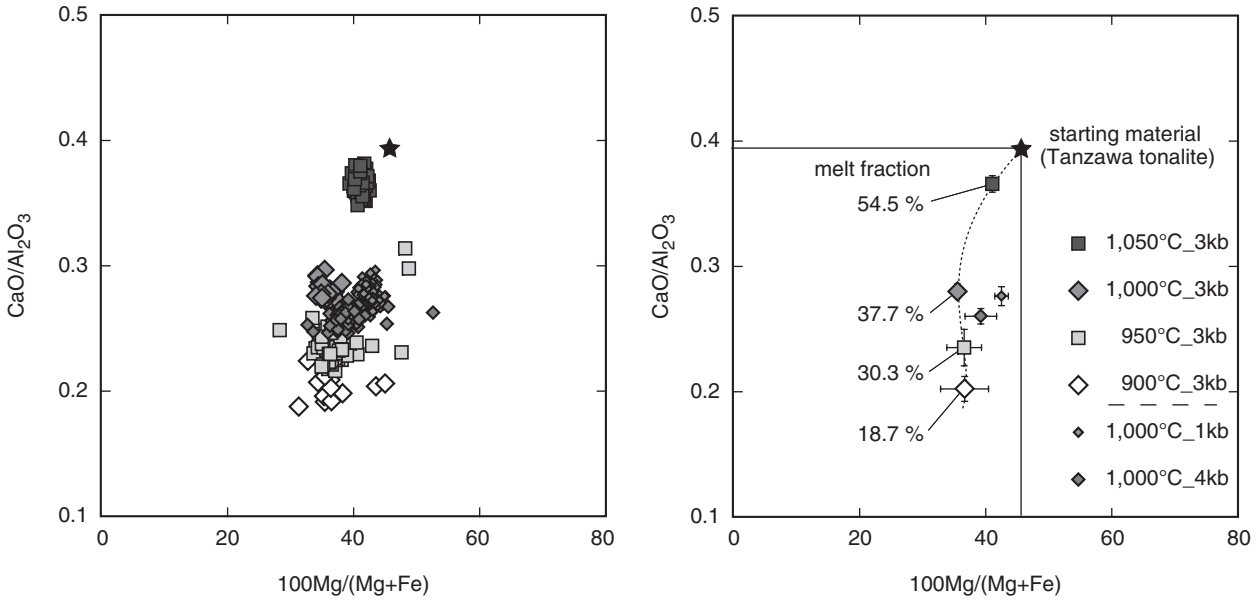

Fig. 15. CaO/Al_2O_3 vs Mg-number of experimental melts of Tanzawa tonalite. CaO/Al_2O_3 increases with temperature and melt fraction, but the Mg-number values of the melts stay fairly constant. Data from Shukuno *et al.* (2006) and T. Suzuki (Electronic Appendix Table 2).

The CaO/Al_2O_3 values of rhyolites from the Izu–Bonin arc range from ~0·1 to ~0·5 (Fig. 4c), with rhyolites from basalt-dominant volcanoes (R1) having the highest CaO/Al_2O_3 ratios and rift-type rhyolites (R3) the lowest. The differences are too large to reflect derivation from the same source. REE patterns (Fig. 5), Zr/Y values, and Sr–Nd–Pb isotope compositions (Fig. 6) also show greater differences between rhyolite types than can be produced from a uniform source. Figure 6 shows that the Sr–Nd–Pb isotope ratios of the R2 rhyolites are closer to Oligocene than Quaternary values (Gill *et al.*, 1994; Taylor & Nesbitt, 1998). Thus, the R1 rhyolites could be derived from Quaternary andesitic sources whereas the R2 rhyolites may be derived from Oligocene sources. R3 rhyolites are most similar to the rift basalts in isotopic composition.

Oligocene vs Quaternary andesite sources in the Izu–Bonin arc

The eruptive products of the Quaternary volcanoes of the Izu–Bonin arc are volumetrically bimodal and andesites are minor in volume (Tamura & Tatsumi, 2002). The same is true for the Oligocene to Pleistocene volcaniclastic deposits and sandstones recovered by ODP drilling in the forearc (Gill *et al.*, 1994; Hiscott & Gill, 1992). The most voluminous rocks in the Tanzawa suite, however, are tonalites with ~60 wt % SiO_2 (Kawate & Arima, 1998); this finding suggests that andesitic compositions are voluminous in the Izu–Bonin arc middle crust. Compositions from 57 to 63 wt % SiO_2, which meet the requirement of the middle crust composition based on seismic velocities (Kodaira *et al.*, 2007*a*), are known from the Quaternary volcanoes (Tamura & Tatsumi, 2002; Tamura *et al.*, 2005, 2007; Shukuno *et al.*, 2006) and Oligocene turbidites (Hiscott & Gill, 1992). Figure 16 shows the variation of FeO*/MgO vs wt % SiO_2 and Mg-number vs wt % SiO_2 for Quaternary andesites and Oligocene andesites. In terms of FeO*/MgO or Mg-number, the Quaternary andesites are about 50% calc-alkaline and 50% tholeiitic, but most Oligocene andesites are calc-alkaline (Fig. 16). The biggest difference is in CaO/Al_2O_3 (Fig. 17). Oligocene andesites (turbidites) have CaO/Al_2O_3 values ranging form ~0·1 to ~0·5, whereas the Quaternary andesites have higher values (0·4–0·6) for both tholeiitic and calc-alkaline varieties. Melting experiments on tonalite (Fig. 15) suggest that different melt fractions (20–40%) have similar CaO/Al_2O_3 (different by only ~0·1). Therefore the difference in CaO/Al_2O_3 between R1, R2 and R3 rhyolites can be attributed to the difference between their Quaternary and Oligocene andesite sources, respectively.

Figure 18 shows the difference between the REE patterns of Oligocene (23–30 Ma) and Neogene turbidites (4–15 Ma) (Gill *et al.*, 1994), and compares them with Quaternary Sumisu andesites (Shukuno *et al.*, 2006). The REE patterns of the Oligocene andesites (turbidites) are flat to slightly LREE-enriched (Gill *et al.*, 1994). As the result of the Shikoku backarc basin formation from 25 to 15 Ma, REE patterns changed to depleted ones in the Quaternary (Gill *et al.*, 1994) (Fig. 18). The REE patterns of Oligocene and Quaternary andesites (turbidites) are almost parallel to those of rhyolites from rhyolite-dominant volcanoes (R2) and rhyolites from basalt-dominant volcanoes (R1) (Fig. 5), respectively.

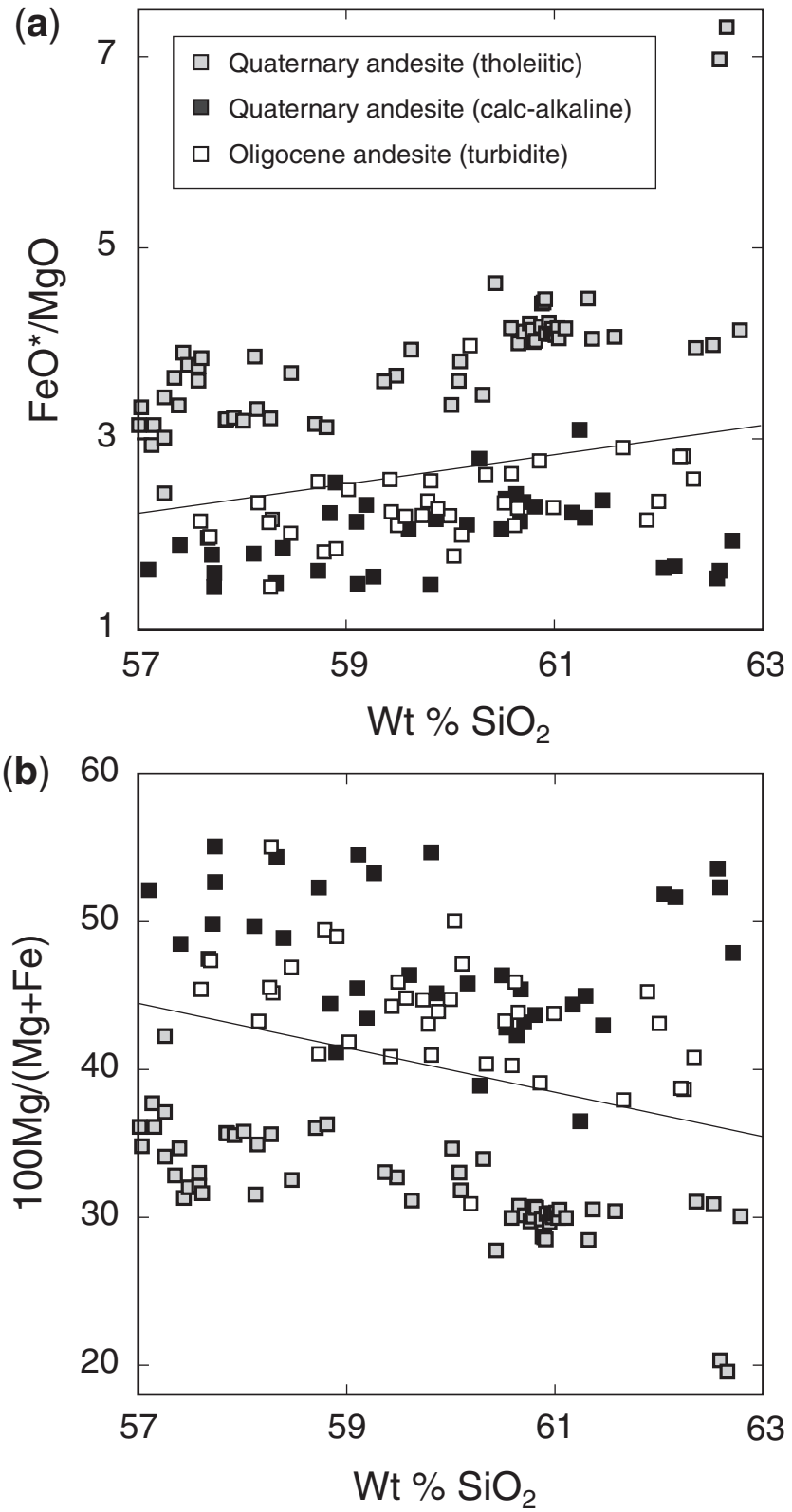

Fig. 16. FeO*/MgO vs SiO_2 (wt %) and Mg-number vs SiO_2 of the Izu–Bonin arc andesites ranging from 57 to 63 wt % SiO_2. Data for Oligocene turbidites are from Hiscott & Gill (1992). Quaternary andesites are from the review by Tamura & Tatsumi (2002) and from Sumisu and Torishima volcanoes (Tamura *et al.*, 2005, 2007; Shukuno *et al.*, 2006). Tholeiitic and calc-alkaline boundary (diagonal continuous line) is after Miyashiro (1974).

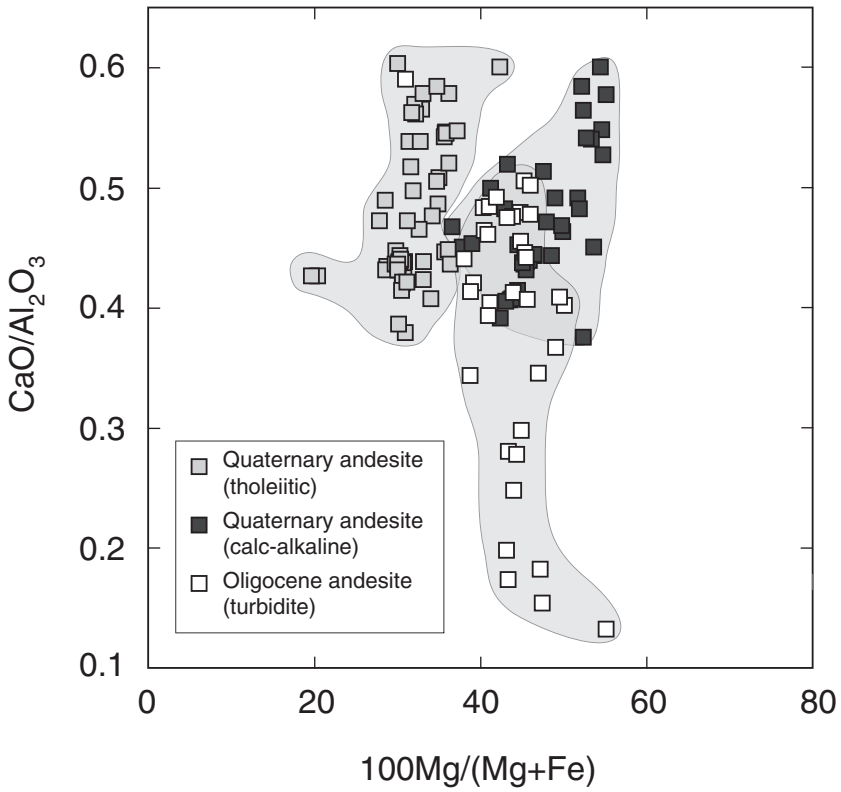

Fig. 17. CaO/Al_2O_3 vs Mg-number for the Izu–Bonin arc andesites (57–63 wt % SiO_2). Oligocene andesites (turbidites) have a wider range in CaO/Al_2O_3 from ~0·1 to ~0·5, whereas both the tholeiitic and calc-alkaline Quaternary andesites have high CaO/Al_2O_3 (0·4–0·6).

Figure 4d shows that there is a significant difference in Zr/Y ratios between rhyolites from basalt-dominant and rhyolite-dominant volcanoes. The Zr/Y ratios of Oligocene andesites (3–4) are also higher than those of Quaternary andesites (2–3). Figure 19 tests the hypothesis that this difference could be caused by variable degrees of partial melting of a dry andesitic source. Zr/Y values in partial melts are estimated by using the modes of residual minerals and melt fractions in the Tanzawa tonalite melting experiments (Shukuno *et al.*, 2006), Zr and Y concentrations of Oligocene andesite (Gill *et al.*, 1994) and Sumisu andesite as sources (Shukuno *et al.*, 2006), and partition coefficients of Zr and Y between dacitic and rhyolitic melt and plagioclase, orthopyroxene, clinopyroxene and magnetite (Ewart & Griffin, 1994). Partial melting of a single source cannot change the Zr/Y ratio by as much as the difference between the R1 and R2 rhyolites. Instead, an increased degree of melting will decrease the Zr/Y ratio by only one unit. Therefore, the systematic difference in Zr/Y between R1 and R2 requires different sources such as Quaternary versus Oligocene basalts and andesites.

Lavas from rhyolite-dominant volcanoes and those from basalt-dominant volcanoes have different Sr, Pb, and sometimes Nd isotope ratios, and R2 and R3 are displaced toward values for the Oligocene arc (Fig. 6). This is consistent with their derivation, at least in part, from older crustal sources. It should be noted that none of the rhyolite types can be derived from Eocene sources, which differ isotopically from younger sources, most notably in Pb and Hf (Pearce *et al.*, 1999; Ishizuka *et al.*, 2006). None of the rhyolites share those distinctive traits. This may indicate that Eocene middle crust does not extend as far west as the current volcanic front.

It is premature to say whether the differences between rhyolite types in Izu apply to other arcs. R1 seem to be more commonly described. For example, rhyolite ignimbrites in Costa Rica share the trace element and isotope ratios of associated basalts (Vogel *et al.*, 2006) as do the 2003 dacites from Anatahan volcano in the Marianas (Wade *et al.*, 2005) and dacites from Raoul Volcano in the Kermadecs (Smith *et al.*, 2006). However, the R2 and R3 types are not found on islands and may await discovery elsewhere.

Differentiation models for rhyolite genesis

The preceding discussion can explain many of the differences between R1 and R2 rhyolites in terms of differences in their andesitic sources in the middle crust. It cannot, however, explain the Sr and Pb isotope ratios of the R2 rhyolites, which are lower and higher than in Oligocene sources, respectively (Fig. 6). Nor can it easily explain the

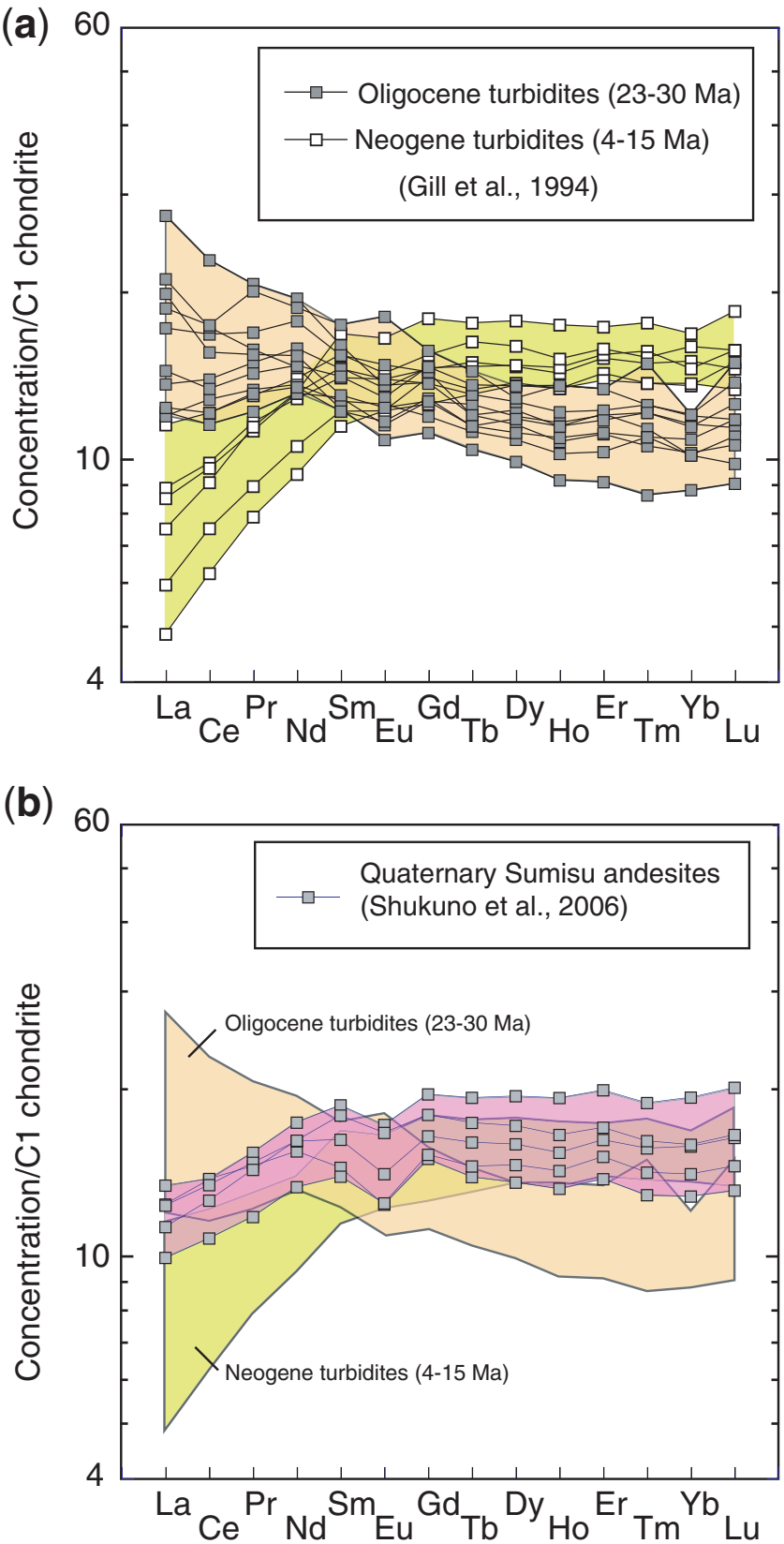

Fig. 18. REE patterns of Oligocene turbidites (23–30 Ma) and Neogene turbidites (4–15 Ma) (Gill *et al.*, 1994) and Quaternary Sumisu andesites (Shukuno *et al.*, 2006). C1 chondrite composition is that of Sun & McDonough (1989). Patterns of Oligocene and Quaternary andesites are almost parallel to Quaternary R2 and R1 rhyolites shown in Fig. 5, respectively.

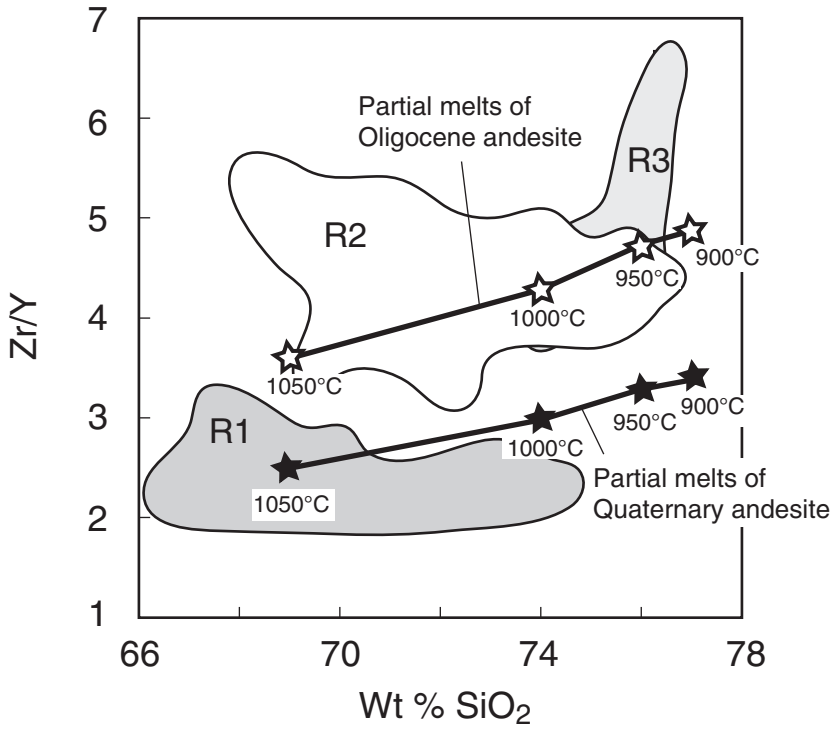

Fig. 19. Zr/Y vs SiO_2 (wt %) of the Izu–Bonin arc Quaternary rhyolites (Fig. 4d) shown by fields (R1, R2 and R3). R1, R2 and R3 are rhyolites from basalt-dominant volcanoes, rhyolite-dominant volcanoes and rift-type rhyolites, respectively. Open and filled stars show Zr/Y vs SiO_2 for partial melts of Oligocene andesite and Quaternary andesite, respectively. Zr/Y values are estimated by using the modes of residual minerals and melt fractions of Tanzawa tonalite melting experiments (Shukuno *et al.*, 2006), and partition coefficients for felsic melt and plagioclase, orthopyroxene, clinopyroxene and magnetite from Ewart & Griffin (1994). Zr and Y concentrations for Oligocene andesites are from Gill *et al.* (1994) and for Quaternary andesites are from Shukuno *et al.* (2006).

abundance of R3 rhyolite in the backarc rifts and extensional zones far from the heat source of the basalt-dominated arc-front volcanoes. The similarities between the R2 and R3 rhyolites is consistent with Oligocene andesitic sources for them both. However, an alternative is that the R3 rhyolites are genetically related to the BAK basalts with which they are spatially associated and share many trace element and isotopic traits. Whether this relationship is via fractional crystallization or partial melting and remobilization is a secondary matter.

Interestingly, the BAK basalts share many trace element and isotopic traits with the Oligocene andesites, including all of the diagnostic differences between the Oligocene and Quaternary rocks used above to argue for different andesitic sources. However, most BAK basalts have lower Sr and Pb isotope ratios and lower Ba/La than most Oligocene rocks. R3 rhyolites share these traits. Therefore, it is hard to exclude BAK basalts as a potential source of R3. R3 rhyolites are widespread across the extensional zone and, therefore, chemically more diverse than R1 and R2. We do not yet have detailed chemical analysis of this diversity nor the age of the rhyolites. Therefore, it is premature to try to identify their source(s) uniquely.

None the less, if R3 rhyolites are related to BAK sources, then there are two implications. First, some Izu rhyolites might have basaltic instead of andesitic sources and be derived by fractional crystallization of basalt instead of partial melting of andesite. However, this would not explain the correlations between volcano type and crustal thickness, which is one of the main points of this study. Second, there should be no R3 rhyolites before BAK first appeared at ~2 Ma (Ishizuka *et al.*, 2003*b*); none are known before that time in ODP cores from the forearc (Gill *et al.*, 1994; Straub *et al.*, 2004).

The above findings and interpretations prompt us to favor the concept that the R1 rhyolites are partial melts of Quaternary andesitic sources in the middle crust, that R2 rhyolites are similarly related to Oligocene andesitic crustal sources, and that R3 rhyolites are derived from BAK basalts either by fractional crystallization or by remobilization within the crust.

RHYOLITE GENESIS AND CRUSTAL EVOLUTION

Geochemically, three types of Quaternary rhyolite exist in the Izu–Bonin arc front, and they are closely related to

volcano type and crustal structure (Fig. 3): rhyolites from basalt-dominant volcanoes (R1), rhyolites from rhyolite-dominant volcanoes (R2), and rift-type rhyolites (R3). R1 rhyolites have the highest CaO/Al_2O_3, which results in higher An content in their plagioclase phenocrysts (Fig. 13). R1 rhyolites have significantly lower Zr/Y and LREE-depleted REE patterns, whereas the latter two have higher Zr/Y and flat to slightly enriched REE patterns. R1 rhyolites have Sr–Nd–Pb isotope compositions similar to Quaternary Izu–Bonin frontal arc basalts, but the latter two rhyolites have significantly lower Sr–Nd–Pb isotope ratios. All of these characteristics of rhyolites from rhyolite-dominant volcanoes and rift-type rhyolites are akin to lavas of both the Oligocene arc and the Plio-Pleistocene backarc extensional zone. We conclude that the crustal source materials of these three types of rhyolites are different. It is not well understood, however, why and how these crustal sources differ systematically and alternate along and behind the Izu–Bonin arc. A new petrological model for the general evolution of arc crust and sub-arc mantle in the Izu–Bonin–Mariana arc–trench system was presented recently (Tatsumi *et al.*, 2008). However, the correlation between smaller scale along-strike crustal variations with a wavelength of ~80 km and their correlation with Quaternary volcano chemistry (Kodaira *et al.*, 2007*a*) are the primary concerns of this study.

Figure 20 is a schematic cross-section for a 100–200 km segment of the Izu–Bonin arc, showing its volcanism and crustal evolution from Eocene–Oligocene to present times. The Eocene–Oligocene crust is assumed to be similar to the thin crust in the Izu–Bonin forearc (Kodaira *et al.*, 2007*b*) (Fig. 20a). Once the arc stabilized near its present location in the Oligocene, locally developed hot regions within the mantle wedge (hot fingers) were responsible for the production of large basaltic volcanoes (Tamura *et al.*, 2002). If these mantle sources remain stationary for millions of years, then basalt-dominant volcanoes will eventually overlie thicker crust (Kodaira *et al.*, 2007*a*) (Fig. 20b). The significant new observation is that basaltic volcanoes overlie thicker middle crust than do rhyolite volcanoes (Kodaira *et al.*, 2007*a*). Remelting of middle crust to form rhyolite magmas takes place beneath both basaltic and rhyolitic volcanoes (R1 and R2 rhyolite, respectively) (Fig. 20c). However, basalt volcanoes consume new middle crust to produce rhyolite magma whereas rhyolite volcanoes consume old Oligocene middle crust. Moreover, rhyolite volcanoes have no mantle roots beneath the crust. Instead, we propose that dikes from the adjacent basalt volcanoes provide the heat source to partially melt the crust.

An important question is whether basaltic magma can be transported laterally for such long distances (10–50 km) from the basalt volcanoes and whether the dikes provide a sufficient heat source. Recently, long-distance lateral magma transport within the crust has been recognized between Izu–Bonin arc volcanoes (e.g. Nishimura *et al.*, 2001; Geshi *et al.*, 2002; Toda *et al.*, 2002; Ishizuka *et al.*, 2008). When Miyake (jima) volcano erupted in 2000, seismic activity began beneath the volcano and migrated about 30 km northwestward for 6 days; this was also accompanied by ground deformation (Nishimura *et al.*, 2001). These events were interpreted to reflect long-distance dike injection from Miyakejima volcano (Geshi *et al.*, 2002; Toda *et al.*, 2002). Another example is from Hachijo volcano. Ishizuka *et al.* (2008) showed geochemically that magma was transported laterally for long distances (>20 km) at a depth of 10–20 km (middle–lower crust) from Hachijo volcano, which resulted in the formation of a 20 km long submarine volcanic chain (Hachijo NW chain). Moreover, seismic reflection profiles of the Izu–Bonin arc crust support the existence of sills under the rhyolite volcanoes. Kodaira *et al.* (2007*a*) found laterally continuous sub-horizontal crustal reflectors within the arc crust along the volcanic front of the Izu arc. Many of these reflectors indicate major crustal layer boundaries that have an abrupt change of velocity gradient. However, other reflectors that cross isovelocity contours (which are labeled x in their fig. 8), were interpreted as floating reflectors representing features such as laterally intruded sills up to 50 km long. These lines of evidence suggest that magma can be transported laterally for long distances (10–50 km) from basalt volcanoes. A forearc Pliocene basalt sill drilled at ODP Site 792 also indicates that magma intruded up to 50 km from a basalt-dominated volcano, Aogashima (Taylor *et al.*, 1995).

Huppert & Sparks (1988) showed that when basalt sills are emplaced into preheated continental crust, or as envisaged here a silicic to intermediate middle crust, a voluminous overlying layer of convecting silicic magma can be produced. Repeated intrusion of dikes or sills from basalt volcanoes could preheat the crust between them, resulting in formation of silicic magmas by melting the 'continental crust' components (middle crust) in the Izu–Bonin arc. Moreover, the amount of crustal melt generated could be high compared with the amount of basalt injected (Huppert & Sparks, 1988).

SW Torishima shows a close relationship between differentiated Torishima basalts, primitive rift basalt (BAK) and R2 rhyolite (Fig. 11). The differentiated Torishima basalts must have transferred more latent heat to the crust through crystallization than the primitive quenched basalts, and they could be the heat source that produced the R2 rhyolites. Such a model of production and consumption of middle crust below basaltic volcanoes and rhyolitic volcanoes, respectively, would explain the dramatic along-strike changes in the thickness of the middle crust over distances <50 km (Fig. 3a). R3 rhyolites could

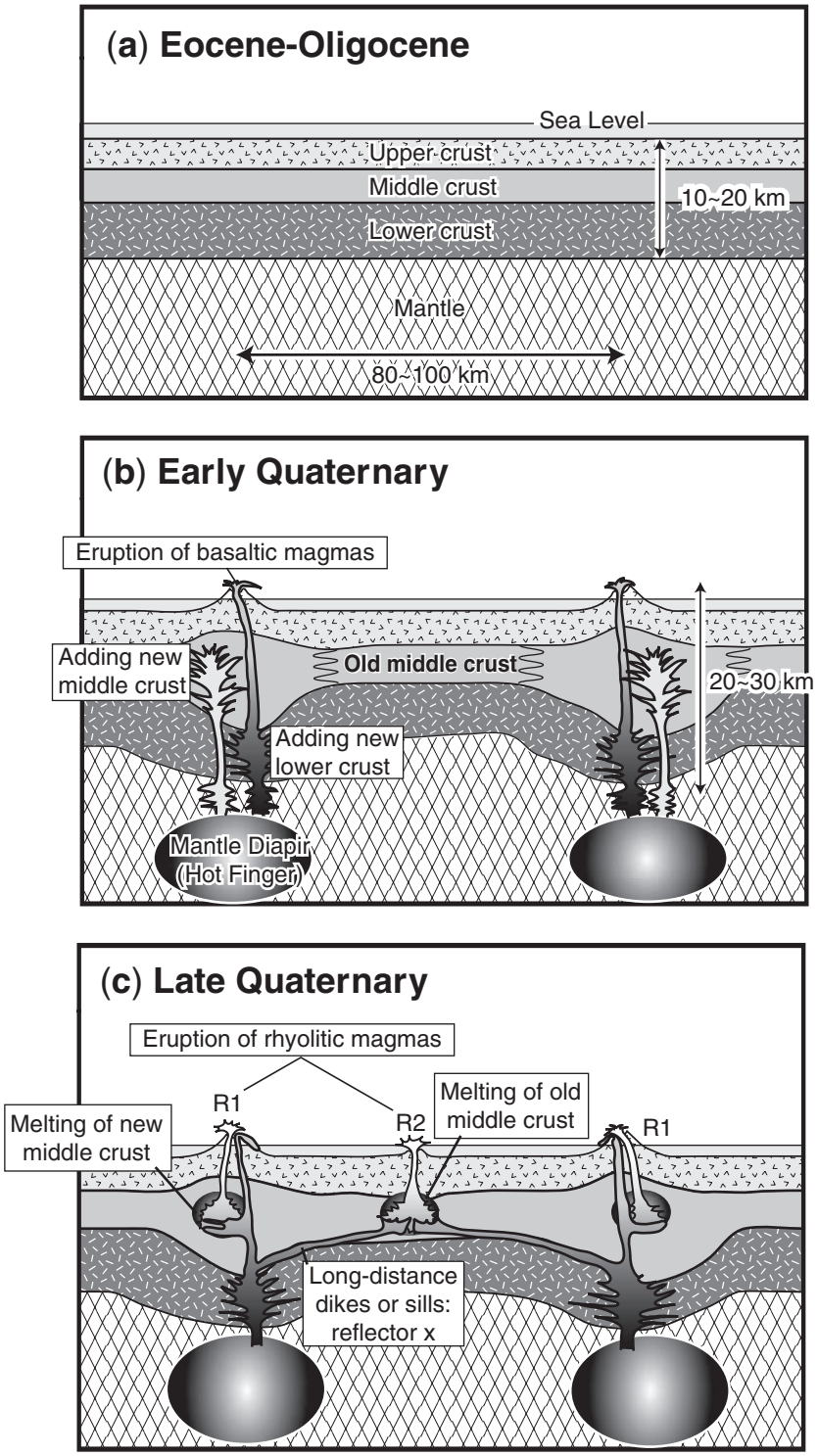

Fig. 20. Schematic along-arc cross-section of the Izu–Bonin arc, showing the location of volcanism and crustal evolution. (a) Eocene–Oligocene. Crustal structure is assumed to be similar to that of the thin crust in the present-day Izu–Bonin arc front (Kodaira *et al.*, 2007*b*). Volcano distribution and variations in crustal thickness in this early stage are not well understood and are omitted. (b) Early Quaternary. Locally developed hot regions within the mantle wedge (hot fingers) are responsible for the location of basaltic volcanoes (Tamura *et al.*, 2002). Basalt-dominant volcanoes have thicker crust (Kodaira *et al.*, 2007*a*) that might have accumulated during Neogene-present times. Black areas represent basaltic magma systems that thicken the lower crust and also erupt to the surface. Grey areas represent magnesian andesite magma systems that thicken the middle crust and do not erupt to the surface because their higher water contents promote rapid crystallization within the crust (Tamura & Tatsumi, 2002). (c) Later Quaternary. Remelting of the middle crust and formation of rhyolite magmas takes place at both basaltic and rhyolitic volcanoes. Basalt intrusions melt new middle crust to produce R1 rhyolite magma at basalt-dominant volcanoes, and melt Oligocene middle crust to produce R2 rhyolite magma at rhyolite-dominant volcanoes. Rhyolite volcanoes have no mantle roots beneath the crust but dikes (reflector x of Kodaira *et al.*, 2007*a*) travel laterally from the basalt volcanoes to produce rhyolite magma having the characteristics of Oligocene middle crust.

be the fractionation products of BAK basalts as discussed above. Another possibility is that both R2 and R3 rhyolites are partial melts of Oligocene middle crust. In this case, the heat source for the R3 rhyolites could be dikes from the frontal basalt-dominated volcanoes and/or the rift basalts from just below.

ACKNOWLEDGEMENTS

This work was supported in part by the NSF MARGINS program, award OCE0325189, the JSPS Grant-in-Aid for Scientific Research (B) (17340165 and 20340122) and Grant-in-Aid for Creative Scientific Research (19GS0211). This work was made possible by the exchange visits of Y. Tamura and J. Gill between IFREE/JAMSTEC and UCSC. We are indebted to Captain F. Saito, the crews of R.V. *Natsushima*, K. Chiba and the operation team of ROV *Hyper-Dolphin* during JAMSTEC NT06-21 cruise. We thank J. Blundy, C. Macpherson and I. Smith for careful and insightful reviews, and J. Gamble for editorial help.

SUPPLEMENTARY DATA

Supplementary data for this paper are available at *Journal of Petrology* online.

REFERENCES

Blundy, J. D. & Sparks, R. S. J. (1992). Petrogenesis of mafic inclusions in granitoids of the Adamello massif, Italy. *Journal of Petrology* **33**, 1039–1104.

Cashman, K. V. & Fiske, R. S. (1991). Fallout of pyroclastic debris from submarine eruption columns. *Science* **253**, 275–280.

Chang, Q., Shibata, T., Shinotsuka, K., Yoshikawa, M. & Tatsumi, Y. (2003). Precise determination of trace elements in geological standard rocks using inductively coupled plasma mass spectrometry. *Frontier Research on Earth Evolution (IFREE Report for 2001–2002)* **1**, 357–362.

Couch, S., Sparks, R. S. J. & Carroll, M. R. (2001). Mineral disequilibrium in lavas explained by convective self-mixing in open magma chambers. *Nature* **411**, 1037–1039.

Davidson, J., Turner, S., Handley, H., Macpherson, C. & Dosseto, A. (2007). Amphibole 'sponge' in arc crust. *Geology* **35**, 787–790; doi:10.1130/G23637A.1.

Ewart, A. & Griffin, W. L. (1994). Application of proton-microprobe data to trace-element partitioning in volcanic rocks. *Chemical Geology* **117**, 251–284.

Fryer, P., Taylor, B., Langmuir, C. H. & Hochstaedter, A. G. (1990). Petrology and geochemistry of lavas from the Sumisu and Torishima backarc rifts. *Earth and Planetary Science Letters* **100**, 161–178.

Geshi, N., Shimano, T., Chiba, T. & Nakada, S. (2002). Caldera collapse during the 2000 eruption of Miyakejima Volcano, Japan. *Bulletin of Volcanology* **64**, 55–68.

Gill, J. B. (1981). *Orogenic Andesites and Plate Tectonics*. New York: Springer, 390 pp.

Gill, J. B., Seales, C., Thompson, P., Hochstaedter, A. G. & Dunlap, C. (1992). Petrology and geochemistry of Pliocene–Pleistocene volcanic rocks from the Izu-arc, Leg 126. In: Taylor, B. & Fujioka, K. *et al.* (eds) *Proceeding of the Ocean Drilling Program, Scientific Results, 126*. College Station, TX: Ocean Drilling Program, pp. 383–404.

Gill, J. B., Hiscott, R. N. & Vidal, Ph., (1994). Turbidite geochemistry and evolution of the Izu–Bonin arc and continents. *Lithos* **33**, 135–168.

Harford, C. L. & Sparks, R. S. J. (2001). Recent remobilisation of shallow-level intrusions on Montserrat revealed by hydrogen isotope composition of amphiboles. *Earth and Planetary Science Letters* **185**, 285–297.

Harmon, R. S. & Gerbe, M.-C. (1992). The 1982–83 eruption at Galunggung volcano, Java (Indonesia): oxygen isotope geochemistry of a chemically zoned magma chamber. *Journal of Petrology* **33**, 585–609.

Hiscott, R. N. & Gill, J. B. (1992). Major and trace element geochemistry of Oligocene to Quaternary volcaniclastic sands and sandstones from the Izu–Bonin arc. In: Taylor, B. & Fujioka, K. *et al.* (eds) *Proceeding of the Ocean Drilling Program, Scientific Results, 126*. College Station, TX: Ocean Drilling Program, pp. 467–485.

Hochstaedter, A. G., Gill, J. B., Kusakabe, M., Newman, S., Pringle, M., Taylor, B. & Fryer, P. (1990*a*). Volcanism in the Sumisu Rift, I. Major element, volatile, and stable isotope geochemistry. *Earth and Planetary Science Letters* **100**, 179–194.

Hochstaedter, A. G., Gill, J. B. & Morris, J. D. (1990*b*). Volcanism in the Sumisu Rift, II. Subduction and non-subduction related components. *Earth and Planetary Science Letters* **100**, 195–209.

Hochstaedter, A. G., Gill, J. B., Taylor, B., Ishizuka, O., Yuasa, M. & Morita, S. (2000). Across-arc geochemical trends in the Izu–Bonin arc: Constraints on soured composition and mantle melting. *Journal of Geophysical Research* **105**, 495–512.

Hochstaedter, A. G., Gill, J. B., Peters, R., Broughton, P. & Holden, P. (2001). Across-arc geochemical trends in the Izu–Bonin arc: Contributions from the subducting slab. *Geochemistry, Geophysics, Geosystems* **2**, 2000GC000105.

Huppert, H. E. & Sparks, R. S. J. (1988). The generation of granitic magmas by intrusion of basalt into continental crust. *Journal of Petrology* **29**, 599–624.

Ikeda, Y. & Yuasa, M. (1989). Volcanism in nascent back-arc basins behind the Shichito ridge and adjacent areas in the Izu–Ogasawara arc, northwest Pacific: evidence for mixing between E-type MORB and island arc magmas at the initiation of back-arc rifting. *Contributions to Mineralogy and Petrology* **101**, 377–393.

Ishizuka, O., Geshi, N., Itoh, J., Kawanabe, Y. & TuZino, T. (2008). The magmatic plumbing of the submarine Hachijo NW volcanic chain, Hachijojima, Japan: long-distance magma transport? *Journal of Geophysical Research* **113**, doi:10.1029/2007JB005325.

Ishizuka, O., Kimura, J.-I., Li, Y. B., Stern, R. J., Reagan, M. K., Taylor, R. N., Ohara, Y., Bloomer, S. H., Ishii, T., Hargrove, U. S., , III & Haraguchi, S. (2006). Early stages in the evolution of Izu–Bonin arc volcanism: New age, chemical, and isotopic constraints. *Earth and Planetary Science Letters* **250**, 385–401.

Ishizuka, O., Taylor, R. N., Milton, J. A. & Nesbitt, R. W. (2003*a*). Fluid–mantle interaction in an intra-oceanic arc: constraints from high-precision Pb isotopes. *Earth and Planetary Science Letters* **211**, 221–236.

Ishizuka, O., Uto, K. & Yuasa, M. (2003*b*). Volcanic history of the back-arc region of the Izu–Bonin (ogasawara). In: Larter, R. D. & Leat, P. H. (eds) *Intra-Oceanic Subduction Systems: Tectonic and Magmatic Processes. Geological Society, London, Special Publications* **219**, 187–205.

Kawate, S. & Arima, M. (1998). Petrogenesis of the Tanzawa plutonic complex, central Japan: Exposed felsic middle crust of the Izu–Bonin–Mariana arc. *Island Arc* **7**, 342–358.

Kitamura, K., Ishikawa, M. & Arima, M. (2003). Petrological model of the northern Izu–Bonin–Mariana arc crust: constraints from high-pressure measurements of elastic wave velocities of the Tanzawa plutonic rocks, central Japan. *Tectonophysics* **371**, 213–221.

Kodaira, S., Sato, T., Takahashi, N., Ito, A., Tamura, Y., Tatsumi, Y. & Kaneda, Y. (2007*a*). Seismological evidence for variable growth of crust along the Izu intraoceanic arc. *Journal of Geophysical Research* **112**, B05104, doi:10.1029/2006JB004593.

Kodaira, S., Sato, T., Takahashi, N., Miura, S., Tamura, Y., Tatsumi, Y. & Kaneda, Y. (2007*b*). New seismological constraints on growth of continental crust in the Izu–Bonin intra-oceanic arc. *Geology* **35**, 1031–1034.

Macpherson, C. G. & Mattey, D. P. (1998). Oxygen isotope variations in Lau Basin lavas. *Chemical Geology* **144**, 177–194.

Matthews, S. J., Sparks, R. S. J. & Gardeweg, M. C. (1999). The Piedras Grandes–Soncor eruptions, Lascar volcano, Chile; evolution of a zoned magma chamber in the central Andean upper crust. *Journal of Petrology* **40**, 1891–1919.

Miyashiro, A. (1974). Volcanic rock series in island arcs and active continental margins. *American Journal of Science* **274**, 312–355.

Miyazaki, T., Takahashi, T., Hirahara, Y., Chang, Q., Vaglarov, B. S., Suzuki, K. & Tatsumi, Y. (2007). Low blank and precise Sr–Nd–Pb analysis and in-situ Sr analysis of minerals in volcanic rocks. *Frontier Research on Earth Evolution (IFREE Report for 2005–2006)* **3**, 72–76.

Murphy, M. D., Sparks, R. S. J., Barclay, J., Carroll, M. R. & Brewer, T. S. (2000). Remobilization of andesite magma by intrusion of mafic magma at the Soufrière Hills volcano, Montserrat, West Indies. *Journal of Petrology* **41**, 21–42.

Nishimura, T., Ozawa, S., Murakami, M., Sagiya, T., Tada, T., Kaizu, M. & Ukawa, M. (2001). Crustal deformation caused by magma migration in the northern Izu Islands, Japan. *Geophysical Research Letters* **28**, 3745–3748.

Nishizawa, A., Kaneda, K., Nakanishi, A., Takahashi, N. & Kodaira, S. (2006). Crustal structure of the ocean–island arc transition at the mid Izu–Ogasawara (Bonin) arc margin. *Earth, Planets, Space* **58**, e33–e36.

Palme, H. & Jones, A. (2004). Solar system abundances of the elements. In: Holland, H. D. & Turekian, K. K. (eds) *Treatise on Geochemistry, 1.* Amsterdam: Elsevier, pp. 41–61.

Pearce, J. A., Kempton, P. D., Nowell, G. M. & Noble, S. R. (1999). Hf–Nd element and isotope perspective on the nature and provenance of mantle and subduction components in Western Pacific arc–basin systems. *Journal of Petrology* **40**, 1579–1611.

Reagan, M. K., Hanan, B. B., Heizler, M. T., Hartman, B. S. & Hickey-Vargas, R. (2008). Petrogenesis of volcanic rocks from Saipan and Rota, Mariana, Islands, and implications for the evolution of nascent island arcs. *Journal of Petrology* **49**, 441–464.

Ryder, C. H., Gill, J. B., Tepley, F., , III, Ramos, F. & Reagan, M. (2006). Closed- to open-system differentiation at Arenal volcano (1968–2003). *Journal of Volcanology and Geothermal Research* **157**, 75–93.

Shukuno, H., Tamura, Y., Tani, K., Chang, Q., Suzuki, T. & Fiske, R. S. (2006). Origin of silicic magmas and the compositional gap at Sumisu submarine caldera, Izu–Bonin arc, Japan. *Journal of Volcanology and Geothermal Research* **156**, 187–216.

Smith, I. E. M., Stewart, R. B. & Price, R. C. (2003). The petrology of a large intra-oceanic silicic eruption: the Sandy Bay Tephra, Kermadec Arc, Southwest Pacific. *Journal of Volcanology and Geothermal Research* **124**, 173–194.

Smith, I. E. M., Worthington, T. J., Price, R. C., Stewart, R. B. & Maas, R. (2006). Petrogenesis of dacites in an oceanic subduction environment: Raoul Island, Kermadec arc. *Journal of Volcanology and Geothermal Research* **156**, 252–265.

Stern, R. J., Fouch, M. J. & Klemperer, S. L. (2003). An overview of the Izu–Bonin–Mariana subduction factory. In: Eiler, J. (ed.) *Inside the Subduction Factory. American Geophysical Union, Geophysical Monograph* **138**, 175–222.

Straub, S. M., Layne, G. D., Schmidt, A. & Langmuir, C. H. (2004). Volcanic glasses at the Izu arc volcanic front: New perspectives on fluid and sediment melt recycling in subduction zones. *Geochemistry, Geophysics, Geosystems* **5**, doi:10.1029/2002GC000408.

Straub, S. M., Schmidt, A., Class, C., Goldstein, S. S. & Gomez-Tuena, A. (2007). Rapid change in the composition of the subducting crust during the early history of the Izu Bonin arc, Pacific NW. In: *Abstracts of Joint NSF-MARGINS and IFREE Workshop: Subduction Factory Studies in the Izu–Bonin–Mariana Arc System: Results and Future Plans*. Available at http://www.nsf-margins.org/IBM07/index.html.

Suga, K. & Fujioka, K. (1990). Volume of volcanic material along northern Izu–Bonin arc. *Bulletin of the Volcanological Society of Japan* **35**, 359–374 (in Japanese with English abstract and figure captions).

Sun, S.-s. & McDonough, W. F. (1989). Chemical and isotopic systematics of oceanic basalts: implications for mantle composition and processes. In: Saunders, A. D. & Norry, M. J. (eds) *Magmatism in the Ocean Basins. Geological Society, London, Special Publications* **42**, 313–345.

Tamura, Y. & Tatsumi, Y. (2002). Remelting of an andesitic crust as a possible origin for rhyolitic magma in oceanic arcs: an example from the Izu–Bonin arc. *Journal of Petrology* **43**, 1029–1047.

Tamura, Y., Koyama, M. & Fiske, R. S. (1991). Paleomagnetic evidence for hot pyroclastic debris flow in the shallow submarine Shirahama Group (upper Miocene–Pliocene), Japan. *Journal of Geophysical Research* **96**, 21779–21787.

Tamura, Y., Tatsumi, Y., Zhao, D., Kido, Y. & Shukuno, H. (2002). Hot fingers in the mantle wedge: new insights into magma genesis in subduction zones. *Earth and Planetary Science Letters* **197**, 105–116.

Tamura, Y., Yuhara, M., Ishii, T., Irino, N. & Shukuno, H. (2003). Andesites and dacites from Daisen volcano, Japan: partial-to-total remelting of an andesite magma body. *Journal of Petrology* **44**, 2243–2260.

Tamura, Y., Tani, K., Ishizuka, O., Chang, Q., Shukuno, H. & Fiske, R. S. (2005). Are arc basalts dry, wet, or both? Evidence from the Sumisu caldera volcano, Izu–Bonin arc, Japan. *Journal of Petrology* **46**, 1769–1803.

Tamura, Y., Tani, K., Chang, Q., Shukuno, H., Kawabata, H., Ishizuka, O. & Fiske, R. S. (2007). Wet and dry basalt magma evolution at Torishima volcano, Izu–Bonin arc, Japan: the possible role of phengite in the downgoing slab. *Journal of Petrology* **48**, 1999–2031.

Tatsumi, Y. & Stern, R. J. (2006). Manufacturing continental crust in the Subduction Factory. *Oceanography* **19**, 104–112.

Tatsumi, Y., Suzuki, T., Kawabata, H., Sato, K., Miyazaki, T., Chang, Q., Takahashi, T., Tani, K., Shibata, T. & Yoshikawa, M. (2006). The petrology and geochemistry of Oto-Zan composite lava flow on Shodo-Shima Island, SW Japan: remelting of a solidified high-Mg andesite magma. *Journal of Petrology* **47**, 595–629.

Tatsumi, Y., Shukuno, H., Tani, K., Takahashi, N., Kodaira, S. & Kogiso, T. (2008). Structure and growth of the Izu–Bonin–Mariana arc crust: 2. Role of crust–mantle transformation and the transparent Moho in arc crust evolution. *Journal of Geophysical Research* **113**, B02203, doi:10.1029/2007JB005121.

Taylor, B. (1992). Rifting and the volcanic-tectonic evolution of the Izu–Bonin–Mariana arc. In: Taylor, B. & Fujioka, K. *et al.* (eds) *Proceeding of the Ocean Drilling Program, Scientific Results, 126.* College Station, TX: Ocean Drilling Program, pp. 627–651.

Taylor, R. N. & Nesbitt, R. W. (1998). Isotopic characteristics of subduction fluids in an intra-oceanic setting, Izu–Bonin arc, Japan. *Earth and Planetary Science Letters* **164**, 79–98.

Taylor, R. N., Narlow, M. S., Johnson, L. E., Taylor, B., Bloomer, S. H. & Mitchell, J. G. (1995). Intrusive volcanic rocks in western Pacific Forearcs. In: Taylor, B. & Natland, J. (eds) *Active Margins and Marginal Basins of the Western Pacific, American Geophysical Union, Geophysical Monograph* **88**, 31–43.

Toda, S., Stein, R. S. & Sagiya, T. (2002). Evidence from the AD 2000 Izu islands earthquake swarm and stressing rate governs seismicity. *Nature* **419**, 58–61.

Vogel, T. A., Patino, L. C., Eaton, J. K., Valley, J. W., Rose, W. I., Alvarado, G. E. & Viray, E. L. (2006). Origin of silicic magmas along the Central American volcanic front: Genetic relationship to mafic melts. *Journal of Volcanology and Geothermal Research* **156**, 217–228.

Wade, J. A., Plank, T., Stern, R. J., Tollstrup, D. L., Gill, J. B., O'Leary, J. C., Eiler, J. M., Moore, R. B., Woodhead, J. D., Trusdell, F., Fischer, T. P. & Hilton, D. R. (2005). The May 2003 eruption of Anatahan volcano, Mariana Islands: Geochemical evolution of a silicic island-arc volcano. *Journal of Volcanology and Geothermal Research* **146**, 139–170.

Wessel, P. & Smith, W. H. F. (1995). New version of Generic Mapping Tools released. *EOS Transactions, American Geophysical Union* **76**, 329.

Wright, I. C., Worthington, T.J. & Gamble, J.A. (2006). New multibeam mapping and geochemistry of the 30°–35° S sector, and overview, of southern Kermadec arc volcanism. *Journal of Volcanology and Geothermal Research* **149**, 263–296.

Yokoyama, T., Kobayashi, K., Kuritani, T. & Nakamura, E. (2003). Mantle metasomatism and rapid ascent of slab components beneath island arcs: Evidence from ^{238}U–^{230}Th–^{226}Ra disequilibria of Miyakejima volcano, Izu arc, Japan. *Journal of Geophysical Research* **108**, doi:10.1029/2002JB002103.

Yuasa, M. & Kano, K. (2003). Submarine silicic calderas on the northern Shichito–Iwojima ridge, Izu–Ogasawara (Bonin) arc, western Pacific. In: White, J. D. L., Smellie, J. L. & Clague, D. A. (eds) *Explosive Subaqueous Volcanism, American Geophysical Union, Geophysical Monograph* **140**, 231–243.